MSc Thesis in Physics

Student: Thomas Langemark Trojahn, cfr686
Field: Computational Biophysics
Title:

Emergent Growth of Intestinal Organoid Crypts from Novel Cell-Polarity Model

Supervisor: Ala Trusina
For questions, feel free to write cfr686@alumni.ku.dk

August 31, 2020

Abstract

From biology it is known that cells are able to self-organize into complex shapes and maintain these shapes even in the presence of a high cell turnover rate. This is especially evident in the intestines, where stem cells proliferate at a high rate and maintain tube-like structures and protrusions. However, little is known as to how these cells are able to do this. For example, how do the protrusions form and how are they able to maintain the stability of the structures in the presence of rapidly dividing cells? This work builds on the 3D cell-polarity model introduced in [13] and aims through the introduction of a set of new dynamics to understand and answer these questions from numerical simulations. The model is a polarized particle approximation in which cells interact as polarized point particles through *apical-basal* (AB) and *planar cell polarity* (PCP) vectors.

We hypothesize that a local WNT3 gradient emanating from a central Paneth cell or cells acts as an *organizing signal* which in turn acts to orient PCP in the surrounding *transit amplifying* (TA) cells and induce crypt formation. I find that with the addition of three main mechanisms, 1) a coupling mechanism which has the effect of orienting PCP due to a local WNT3 gradient generated from cell divisions, 2) differential adhesion to model the adherence properties of Paneth cells and stem cells to their surroundings and 3) a mechanism which models the diffusion of WNT3 through cell-cell contact, it is possible to induce emergent crypt growth that is stable and qualitatively similar to crypts from in-vitro organoids [18]. Crypts are also quantitatively similar to in-vivo crypts from 3-week old laboratory mice [2].

Acknowledgements

Contents

1 Introduction

1.1 Motivations

The mammalian intestines constitute some of the most interesting cellular systems in biology in terms of complexity, morphology and regenerative behaviours and self-organization. The intestinal tract ensures proper uptake of the essential nutrients and building blocks that enable the mammalian organisms to function and grow. The intestinal crypts, Figure 1 **C**, are small protrusions of the small and large intestines positioned in between the villi, the cellular structures that ensure nutrient uptake. The schematic in Figure 1 illustrates parts of the intestinal system that we set out to model in this work.
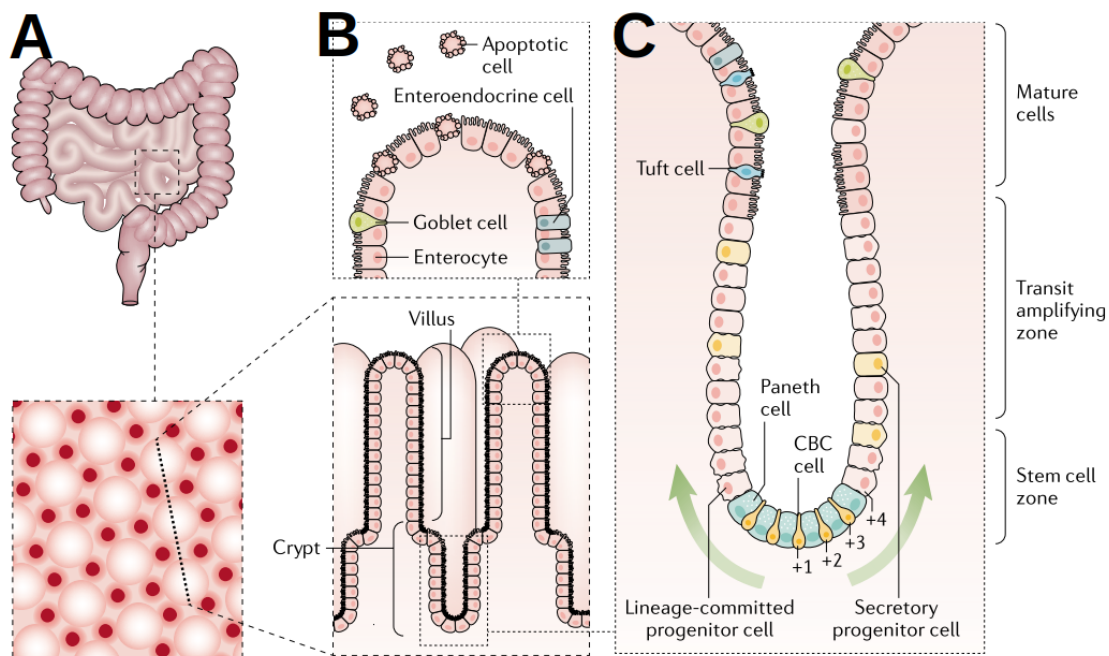
Figure 1: **The stem cell niche**. *From [4], Clevers et al., 2019. Bottom part of* **A** *shows the hexagonal crypt-villus system from the top, with the dark red spots representing the intestinal crypts shown in* **C**. *Note the mixed state of stem cells (CBC cells) and Paneth cells at the bottom of the crypt. This smaller subsystem is usually called the stem cell niche.*

The intestinal crypts are characterized by being populated by a wide variety of different cells that all serve different purposes. Paneth cells in particular are thought to be important for several reasons, one being maintaining the intestinal crypts by protecting the surrounding Lgr5 stem cells (CBC cells) that are responsible for the continued proliferation and replenishment of a variety of intestinal cells by secretion of antimicrobial granules [4]. Paneth cells also secrete WNT3 proteins which bind to so-called *Frizzled* membrane receptors in the stem cells. These WNT3 proteions are known to regulate

directionality in planar cell polarity (PCP) in vertebrates [6] and the gradient of WNT3 is believed to control the spatial structure of the gut epithelium [17]. The complexity of the system shown in Figure 1 is not to be taken lightly. During early development, the system exhibits some very interesting behaviours. For example, the intestines grow by doubling the crypts in a process called *crypt* , where one crypt can split into two. The exact process is not completely understood, but studies have shown that crypt fission is probably initiated when Paneth cell-rich regions are separated by small clusters of Lgr5 stem cells [9].

Even though a plethora of phenomena associated to this system is known in the literature, it is not fully understood what biological processes drive the formation of the crypt-villus system in-vivo. The same is true for the morphological development of the intestinal crypts, which is the focus of this work. In this work we aim to answer the questions

<div align="center">

How does crypt shape emerge?
What determines the shape of the crypts?
How is shape maintained at high cell turnover?

</div>

Part of answering these questions is to investigate minimal in-vitro systems in the laboratory by growing cell cultures derived from intestinal stem cells, as they do in the BRIC group. These minimal in-vitro systems are referred to as *intestinal organoids*. In this work we numerically investigate these systems through the use of a novel cell polarity model which I expand using the hypothesis of an *organizing signal* as explained in a later section. First, however, I will introduce the reader to intestinal organoids as well as other model results that have important parallels to this work. I will then end this section with an introduction of the mechanisms believed to be responsible for the spreading of the organizing signal.

1.1.1 Intestinal Organoids Grown in the Laboratory

After the authors of the seminal paper [15] in 2009 introduced a method by which organoids can be grown in the laboratory, the field of intestinal organoid research is at a point where laboratories around the world are able to consistently grow intestinal organoids from *single* isolated in-vivo stem cells. These cells come from predominantly mice, chicken, pig or human tissues. It is known from experiments that these single isolated intestinal stem cells on their own can proliferate and form what the authors in [18] call *enterocysts*. These enterocysts are spherical cell structures comprised of enterocytes, a specialized cell type which is responsible for the nutrient uptake. This cell type can be seen in Figure 1 **B**. Both the budding organoid and the enterocyst have an internal lumen, i.e. an inside, which in the intestinal system would correspond to the inside of the intestinal wall. After a period of cell divisions where the system reaches the enterocyst state as shown on the right in Figure 2, a symmetry breaking event is then observed in which a fraction of the enterocyst cells differentiate into Paneth cells.

This then leads to the formation of more stem cells and protrusions at the site of the Paneth cells after the Paneth cells' secretion of WNT3. This can be seen on the left in Figure 2, where the Paneth cells lead to the blue protrusions.
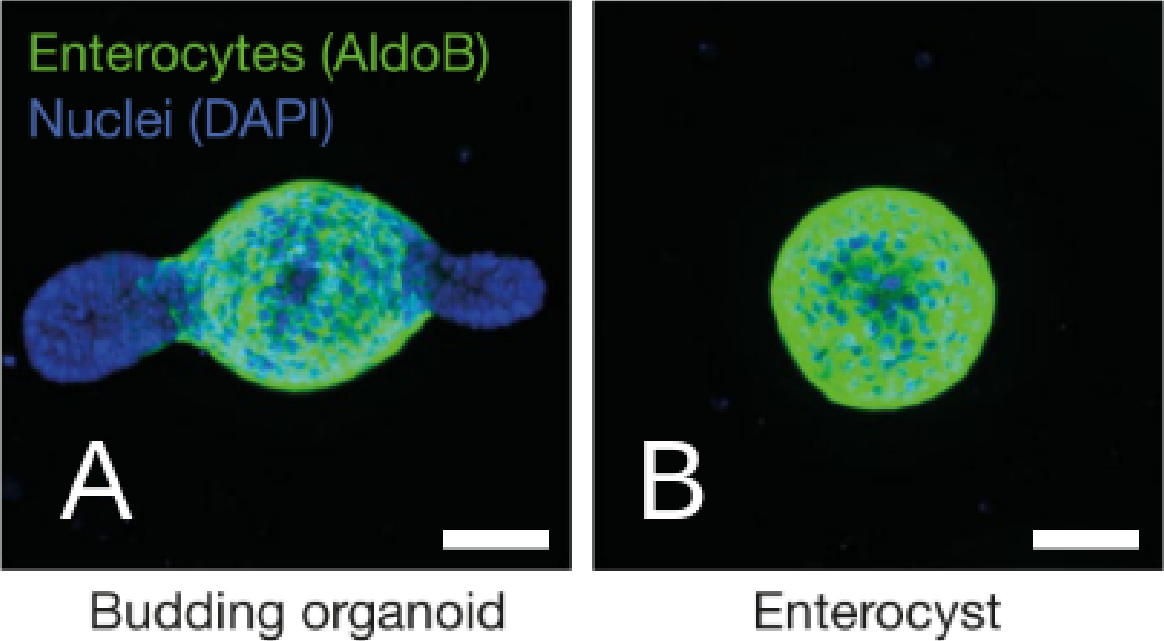
Figure 2: **Laboratory-grown organoids**. *From [18], Serra et al., 2019. The budding organoid in subfigure **A** and the enterocyst in subfigure **B**. The blue protrusions in **A** are crypts like the one seen in Figure 1 **C**.*

1.1.2 Parallels from Previous Models

Variants of the original model and the original model itself [13], introduced in Section 1.2, show the ability to induce tubologenesis and formation of vascular networks [7] and early stages of organogenesis [11]. *This makes clear to us that PCP plays a pivotal role in tube formation in these systems.* Furthermore, we believe that WNT3 proteins are intimately connected to these mechanisms, since it is known that WNT is one of the signalling proteins involved in the PCP pathways [20]. Figures 3 and 4 illustrate how in [11] the authors initialize PCP in the plane to "swirl" tangentially around what is to become the central axis of the budding tube. This swirling of PCP vectors is then maintained and leads to the protrusion of the tube. This swirling of PCP vectors will serve as a starting point when I set out to model the crypt formation due to the WNT3 organizing signal.
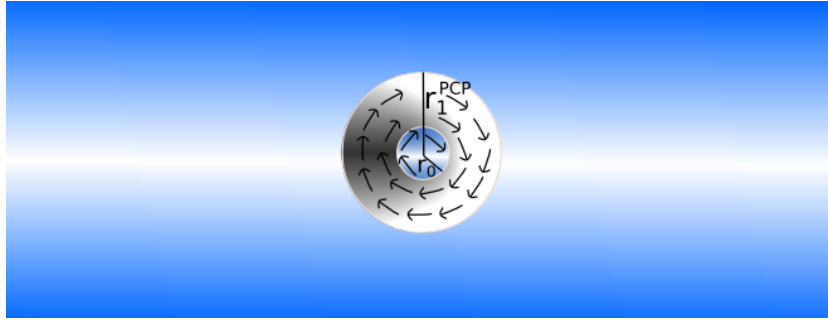
Figure 3: **Initial configuration of the cell sheet for budding and budding sheet**. *From [11], Nielsen et al., 2020. PCP is initialized on a ring in the plane, with the direction of PCP tangential to the tube axis.*
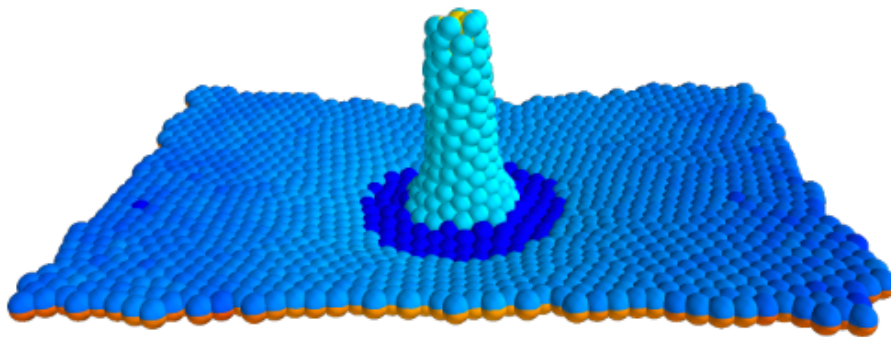
Figure 4: **The initial configuration of PCP leads to a tube budding out of plane**, *with the cells that make up the tube having the same orientation of PCP tangential to the tube axis. Blue and orange colors in the plane indicate AB-polarity.*
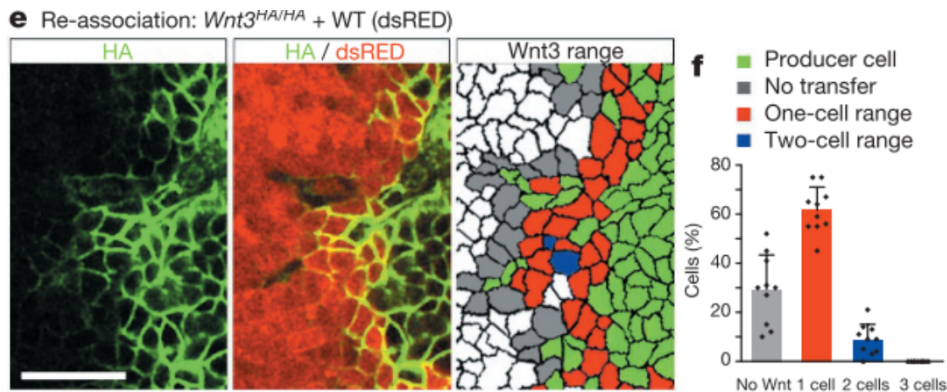
Figure 5: **The transfer of WNT3 has limited range and is most likely due to cell divisions**. *From [3], Farin et al., 2016. Figures show the range of WNT3 transfer to be limited to 1-2 cells away from the Paneth cells and thus this paper concludes that the gradient arises because of stem cell divisions. Paneth cells are green.*

1.1.3 Experimentally Observed WNT3 Gradients

The hypothesized role of WNT3 as an organizing signal naturally leads to questions of the importance of the shape of the distribution of WNT3, in the following called the WNT3 gradient. In Figure 6 it is hinted that the gradient is linear. However, this is not clear from the article. In order to model the system we thus require experimental data of the shape of the WNT3 gradient. However, little is known about the shape of the gradient but some information does exist. It is known that WNT3 exhibits poor solubility, why it is therefore believed that the observed WNT3 gradients are primarily due to spreading by cell divisions or direct cell-cell contact [3, 4].

One can imagine that when stem cells divide, a fraction of the membrane-embedded Frizzled receptors (i.e. the receptors that bind WNT3 proteins) and thus the bound WNT3 proteins are passed on to the newly created cells, thereby creating the observed gradient. This mechanism is suggested in Figure 5, where the key observation is that WNT3 only spreads out 1-2 cells away from the Paneth cells, supporting the idea of cell divisions or cell-cell contact as the driving mechanism for the establishment of the WNT3 gradients.

1.1.4 Paneth-Secreted WNT3 to PCP Coupling Hypothesis

The main hypothesis of this work is that a gradient of WNT3 which emanates from the WNT3-secreting Paneth cells acts as an organizing signal so as to orient PCP in the transit amplifying (TA) zone to induce crypt formation.
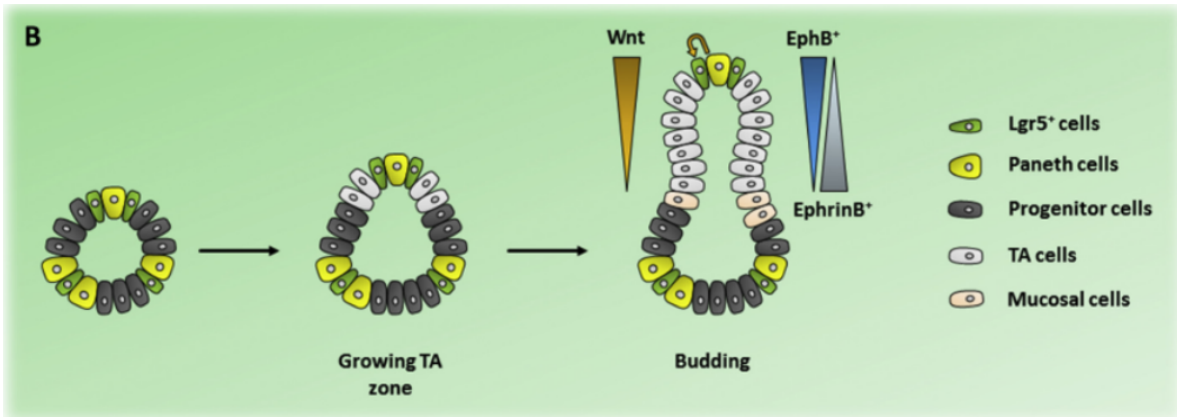
Figure 6: **Overview of enterocyst to budding organoid transition***. From [10], Merker et al., 2016. Note how the gradient of WNT is strongest at the base of the budding crypt. The budding starts at the site of the Paneth cell.*

It is known through the work on the canonical and non-canonical WNT signalling pathways in vertebrates that WNT is one of the signalling proteins involved in the

PCP pathways [20]. It has also been shown that perturbations of the WNT signalling pathway in *Xenopus* aquatic frogs have resulted in the loss of convergent extension (CE), i.e. cell movement, and cell polarization [12], all mechanisms linked to tube formation.

Figure 6 shows an example of how WNT3 secreted by Paneth cells amongst other signalling proteins act together to induce stem cell proliferation and differentiation [10]. *The preceding considerations makes it clear to us that it is important to investigate whether or not it is possible to expand the original model [13] in order to induce crypt formation as it is observed in intestinal organoids through the orientation of PCP due to WNT3.*

1.2   The Original Model

The model build upon in this work was introduced in the original paper [13]. This model is a 3D model with cells treated as polarized point particles. Each cell has associated with it two types of polarities represented as unit vectors, see Figure 7, and the vectors of one cell interacts with the vectors of its Voronoi-neighbour cells through a pairwise interaction determined by a potential function. The two types of polarities in the model are apical-basal (AB) and planar cell polarity (PCP). These two vector quantities represent cell-cell adhesion proteins that govern directionality, and as such they represent a form of symmetry breaking when they are introduced in an aggregate of cells with no initial preferred symmetries.

The inter-particle Lennard-Jones-like potential with the two polarity vectors is defined for cells i and j as

$$V_{ij} = e^{-r_{ij}} - Se^{-r_{ij}/\beta}, \quad S = \lambda_1 S_1 + \lambda_2 S_2 + \lambda_3 S_3. \tag{1}$$

The total potential energy of a cell i is the sum of the neighbour-interactions, i.e.

$$V_i = \sum_j V_{ij}. \tag{2}$$

The motions of the individual cells and their associated polarity vectors are then calculated based on derivatives of this potential assuming overdamped Langevin dynamics:

$$\frac{d\vec{r_i}}{dt} = -\frac{dV_i}{d\vec{r_i}} + \eta \tag{3}$$

$$\frac{d\vec{p_i}}{dt} = -\frac{dV_i}{d\vec{p_i}} + \eta \tag{4}$$

$$\frac{d\vec{q_i}}{dt} = -\frac{dV_i}{d\vec{q_i}} + \eta. \tag{5}$$

9
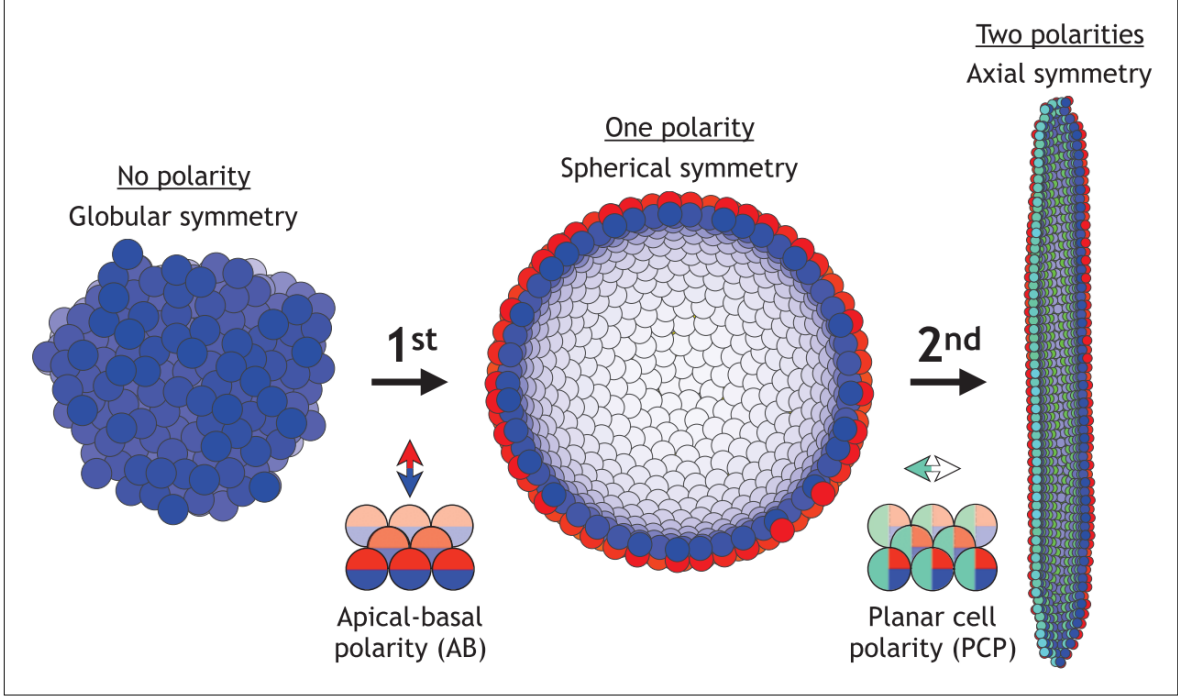
Figure 7: **Introduction of symmetries shape an aggregate of cells**. *From [13], Nissen et al., 2018. Introduction of the first AB polarity to an aggregate of cells leads to spherical symmetry, whereas introduction of the second PCP polarity leads to axial symmetry and formation of tubes.*

All vectors are then subsequently normalized to unity and time is progressed by a simple Euler integration with $dt = 0.1$. If $S = 1$ cells are maximally attracted and if $S = -1$ cells are maximally pushed away from eachother, see Figure 8. $\hat{r}_{ij}$ is the unit vector that points from cell i to cell j. β is a parameter that sets the inter-particle equilibrium distance (equal to 2 when also $\sum_i \lambda_i = 1$). Throughout this work this has the value $\beta = 5$, same as in [13]. η is an uncorrelated Gaussian noise centered around $\sigma_\eta = 0.1$. The $\lambda_i's$ are scalars that set the strengths of the specific interactions and each of the $S_i's$ are unit vector cross products, which for convenience have been written out below using the quadruple product rule:

$$S_1 = (\hat{p}_i \times \hat{r}_{ij}) \cdot (\hat{p}_j \times \hat{r}_{ij}) = (\hat{p}_i \cdot \hat{p}_j) - (\hat{p}_i \cdot \hat{r}_{ij})(\hat{p}_j \cdot \hat{r}_{ij}) \tag{6}$$

$$S_2 = (\hat{p}_i \times \hat{q}_i) \cdot (\hat{p}_j \times \hat{q}_j) = (\hat{p}_i \cdot \hat{p}_j)(\hat{q}_i \cdot \hat{q}_j) - (\hat{p}_i \cdot \hat{q}_j)(\hat{p}_j \cdot \hat{q}_i) \tag{7}$$

$$S_3 = (\hat{q}_i \times \hat{r}_{ij}) \cdot (\hat{q}_j \times \hat{r}_{ij}) = (\hat{q}_i \cdot \hat{q}_j) - (\hat{q}_i \cdot \hat{r}_{ij})(\hat{q}_j \cdot \hat{r}_{ij}). \tag{8}$$

Here, the unit vectors $\hat{p}_i$ and $\hat{p}_j$ are the AB-polarity vectors for cell i and cell j, respectively, when calculating the pairwise interactions. These computations are done for all

cells in the model using PyTorch[3]. Taken as a whole, the above interactions make it energetically favorable for the system to maximize S, since this minimizes the potential. This will make cells position themselves such that PCP vectors of neighbour cells are as parallel as possible, vice versa for AB vectors. This would have cells attract eachother. Cells would also attract if a cell i had its PCP vector orthogonal to its neighbour cell j's AB vector. Figure 8 illustrates the tendency of cells to attract or repulse given the AB / PCP orientations of interacting cells as well as when cells are Voronoi-neighbours or not.
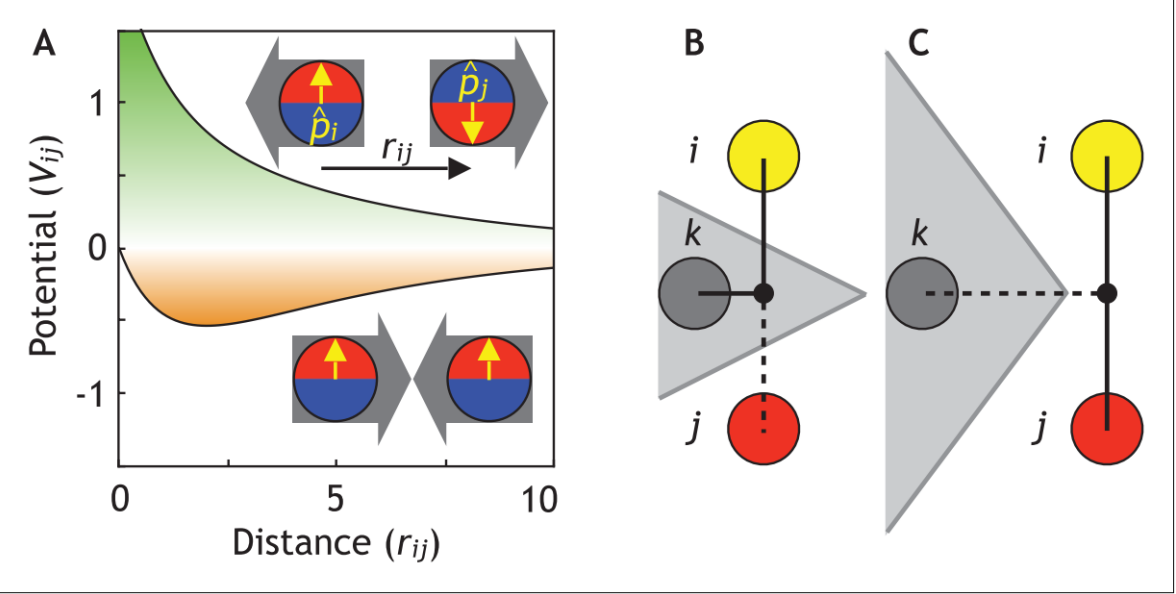
Figure 8: **Pairwise potentials and definition of a nearest neighbour**. *From [13], Nissen et al., 2018.* **A** *Interaction potential.* **B** *Cells i and j are not Voronoi-neighbours since they do not have a direct line-of-sight.* **C** *Cells i and j are no longer obstructed by cell k and are Voronoi-neighbours.*

The above interactions are able to create emergent and robust, complex self-organizing and self-healing structures with interesting morphologies. The resulting shapes are of course dictated by the potential energy, and this minimizes over time, as also discussed and shown in [13], as the cell polarities orient themselves according to Eqs. 6, 7, 8. Resulting shape is also a result of the strength of AB versus PCP interactions, i.e. the value of the λ_i's, with stronger AB interactions favoring spherical structures and stronger PCP interactions favoring tubular structures[4]. The fact that this model is able

---

[3]PyTorch is a fast Python library implemented in C++ mainly for constructing and training e.g. neural networks, much like TensorFlow. It enables calculations to be done on GPU with relative ease and gain of computational speed rather than on CPU, which tend to be much slower.

[4]For more figures and data from [13], see `https://elifesciences.org/articles/38407/figures`. Note that in this paper the authors also investigate how the morphologies develop in the presence of pressure from e.g. a growth medium.

to produce emergent morphologies is especially noteworthy since many cell models use fixed arrays and geometries that only allow for certain types of cell movements, e.g. [8, 1]. These models, however, better capture the details of cell dynamics as compared to this work. The difference in morphological constraints, though, is the main reason that we want to build on top of the original model [13] to simulate intestinal organoid growth in 3D. However, this is not the first model to do this. Other 3D models in the field of intestinal organoids do exist, e.g. [21], but these again rely on an underlying structure to give the overall morphologies and do not as we do allow for emergent morphologies.

2 Results

2.1 Intestinal Organoid Model

In the following sections I will introduce the three main[5] results that lead to crypt formation, i.e. WNT3 to PCP coupling mechanism, differential adhesion and cell-cell contact diffusion of WNT3. When applied in combination, these three mechanisms allow for the formation of crypts similar to the one illustrated in Figure 9.
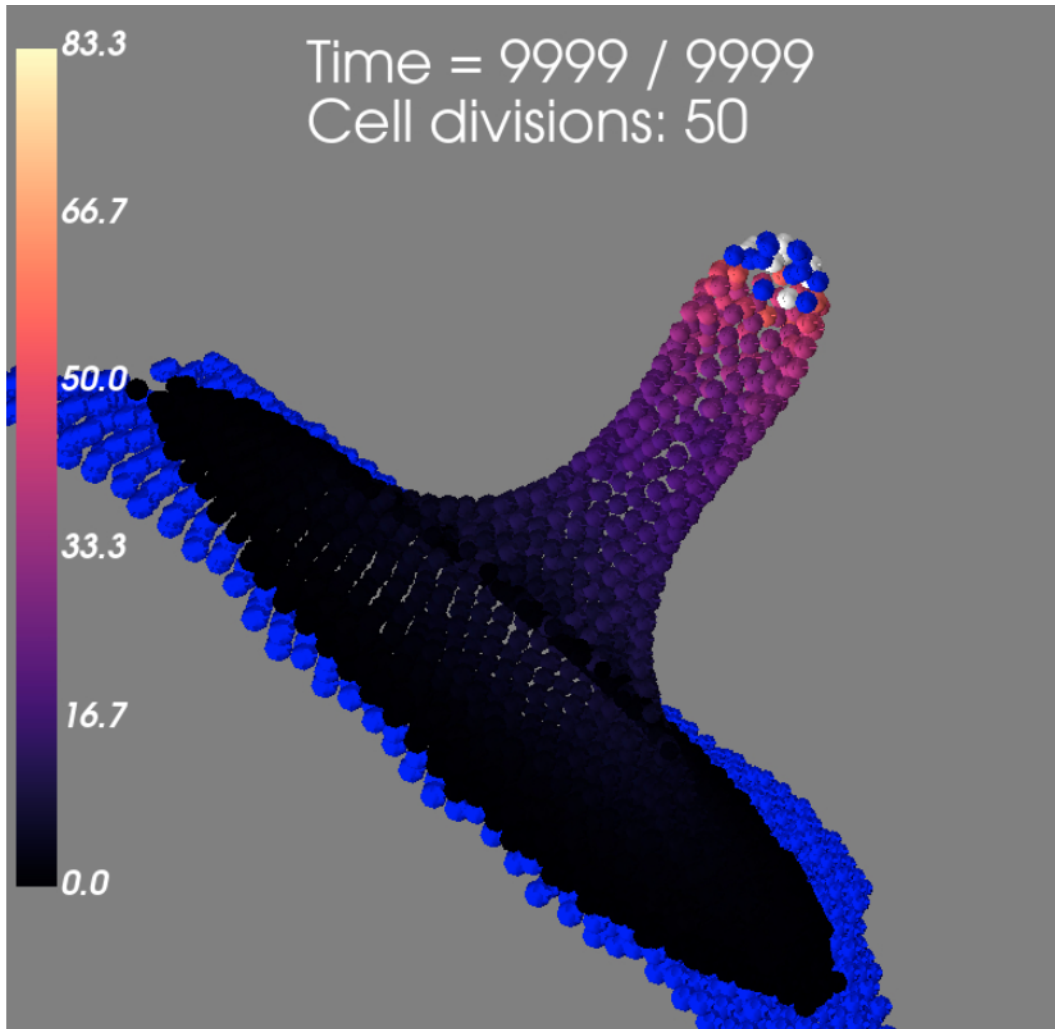
Figure 9: **Crypt grown from plane of cells with patch of mixed Paneth cells and stem cells at crypt base**. *Parameters given in Table 1 and Table 2. Isotropic wedging is on for Paneth cells, see Appendix.*

---

[5]Other mechanisms are also taken into account, e.g. the direction of division being determined by the gradient as well as isotropic apical-basal constriction (wedging) of the Paneth cells. For details into these mechanisms, see the Appendix.

During the initial work I chose to use the parameters used in [13, 11, 7], i.e. for the interactions that are also present in the original model.
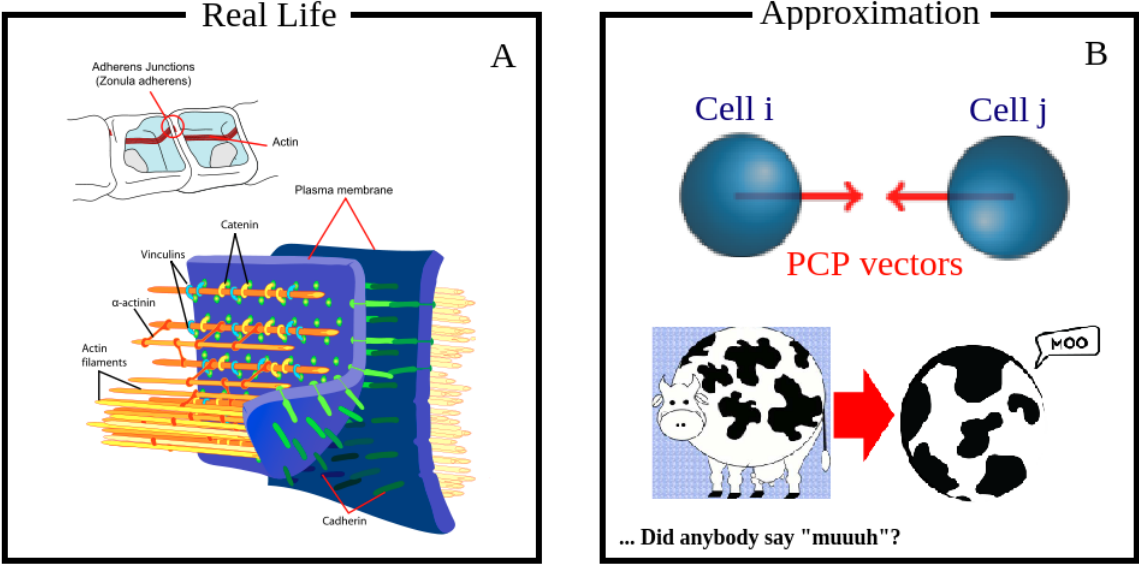
Figure 10: **Adherens junctions are protein complexes that bind cells together at the membranes, figure A. These are modelled as PCP vectors and must be allowed to point in opposite directions, B.** *Cells are treated as point particles.*

We chose to model Eq. 7 and 8 nematically, since two PCP vectors should not be restricted to only point in the same direction. This is because the cell-cell adherens junctions[6] are also approximated by the PCP vectors and these should be allowed to point in opposite directions along the same line.

Thus, the model is made to incorporate the absolute values of Eq. 7 and 8 such that

$$S = \lambda_1 S_1 + \lambda_2 |S_2| + \lambda_3 |S_3|. \tag{9}$$

This will be our starting point.

---

[6]Figure 10 A is from `https://en.wikipedia.org/wiki/Adherens_junction`

2.1.1 WNT3 to PCP Coupling Scheme

Going back to the questions posed in the introduction, this section relates to the first two questions

How does crypt shape emerge?
What determines the shape of the crypts?

In order to understand this I now introduce the main results of this work which is the coupling scheme by which PCP orients itself to the WNT3 gradient. I implement a WNT3 gradient *field* where cells i have associated with them a scalar w_i mimicking WNT3 levels. To interact with this w-field, we introduce a gradient unit vector $\hat{G}_i$, associated to all cells i that are affected by the local gradient of WNT3. See also Figure 11.

$$\vec{G}_i = \sum_j (w_i + w_j) \cdot \hat{r}_{ij}. \tag{10}$$
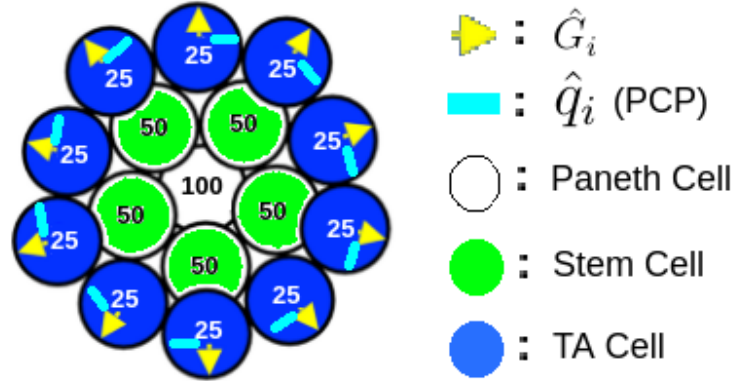
Figure 11: **Example of how a w scalar field might look like for the three cell types. PCP vectors are orthogonal to gradient vectors, $\hat{G}_i$, due to Eq. 11**. *The central Paneth cell has maximum WNT3, throughout the work set at $w_0 = 100$. In this example, stem cells have $w_i = 50$ and TA cells have $w_i = 25$. The yellow arrows represent the gradient vectors pointing away from the source of WNT3 and the light blue line segments represent PCP.*

The vector $\hat{G}_i$ points in the negative direction of the gradient based on the w-field of the local neighbourhood and away from the source of WNT3. The sum in Eq. 10 is taken over all Voronoi-neighbours j to cell i. This vector is subsequently normalized to unity at each step of the simulation for use in Eq. 11, which has the effect of trying to

make the PCP vectors of the WNT3-sensing cells (i.e. cells with $w_i \neq 0$) orthogonal to the their gradient vector $\hat{G}_i$.

We introduce the coupling scheme as an additional term to Eq. 9, namely the S_4 interaction:

$$S_4 = (\hat{q}_i \times \hat{G}_i) \cdot (\hat{q}_i \times \hat{G}_i) = 1 - (\hat{q}_i \cdot \hat{G}_i)^2 \tag{11}$$

This new term of course comes with a new parameter to control the strength of the interaction, λ_4. This is a scalar as the other interaction parameters and the full equation for S in the potential that governs the particle motions is now

$$S = \lambda_1 S_1 + \lambda_2 |S_2| + \lambda_3 |S_3| + \lambda_4 S_4 \tag{12}$$

The interactions over time will tend to minimize the potentials through adjusting cell positions such that PCP vectors $\hat{q}_i$ are orthogonal to gradient vectors, $\hat{G}_i$. This happens because the potential is minimized when S, Eq. 12 is maximized. The new relation Eq. 11 is maximal when $\hat{q}_i \perp \hat{G}_i$ and minimal when $\hat{q}_i$ is parallel or anti-parallel with G_i. See Figure 12 for a visual explanation of the relation between S_4 and the modified potential.
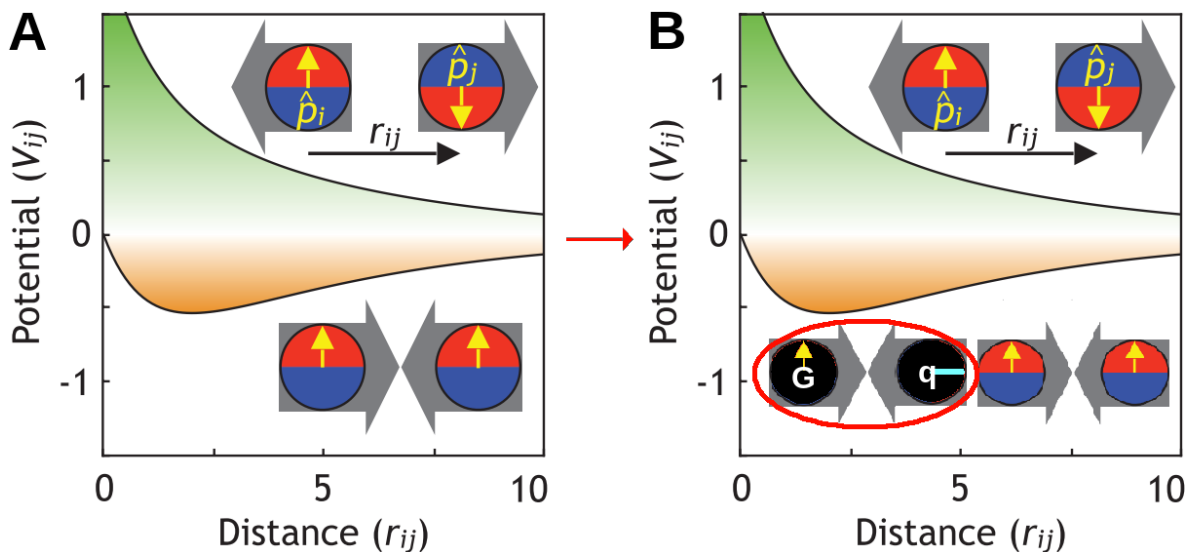
Figure 12: **Modified potential, B, is minimized when gradient vectors G are perpendicular to the PCP vectors q. and cells maximally attract.** *Original potential* **A** *from [13], Nissen et al., 2018. Modified potential* **B** *with new interaction S_4 enclosed in the red ellipse.*

The reason why this mechanism relates to the questions of emergence of the crypt shape and how the shape is determined is because of the way in which the protrusion forms due to the orientation of PCP vectors. As described in the introduction, the authors of [11] are able to get a protrusion by explicitly fixing the orientation of PCP vectors in a swirl, Figure 3 and 4. We effectively have the same situation, but without explicitly fixing the orientation. *Instead, the orientation of PCP depends on the emerging WNT3 gradient and happens by virtue of the modified potential.* The size of the initial swirl, in effect determined by the strengths of interaction scalars λ_2, λ_3 and λ_4, helps to set the width of the protruding crypts. Specifically, we see that λ_3 shows a clear trend with increasing tube width associated to lower values. For details of how these parameters relate to crypt metrics, see the Model Analysis. For detailed explanations and figures of the cell division mechanism as well as other methods used, see the Appendix.

Eqs. 10, 11 and 12 represent the main results of this work.

2.1.2 Differential Adhesion

In order to replicate the mixed pattern of stem cells and Paneth cells at the crypt base, as shown in Figure 1 **C** in the introduction and Figure 13, we chose to also implement *differential adhesion* as discussed by the authors in [9]. This is because Paneth cells show greater adherence to their surroundings than other cell types in the crypt. We chose to implement this difference in adhesion by introducing the symmetric differential adhesion matrix M, Eq. 13, and this mechanism relates to the question,

How is shape maintained at high cell turnover?

One of the difficult aspects of this work has been to achieve a set of dynamics that allow for the mixed salt and pepper-like pattern of stem cells and Paneth cells to persist in the presence of stem cell proliferation. The problem is that cell divisions have the potential to break apart the salt and pepper pattern when daughter stem cells are placed next to their mothers since these new cells can then push out other cells. In my investigations, it turned out that the stability of the salt and pepper pattern is highly dependent on stem cell division rate, i.e. for faster dividing stem cells the patterns tend to break apart more easily. Stem cells are defined based on their local neighbourhood composition. If at least 60% of a cell's neighbours are either stem cells or Paneth cells then the cell becomes a stem cell. Paneth cells cannot change their cell fate. Cell divisions are implemented by choosing a random stem cell every 200 steps which then splits into two new cells.

Each individual element in M represents the value of λ_1 in Eq. 12 for a given cell-cell pair interaction, with the two subscripts indicating the two cell types. The three different cell types are stem cells, Paneth cells and TA cells, represented as types 1, 2 and 3, respectively. For instance, the strength of the S_1 interaction for a Paneth cell
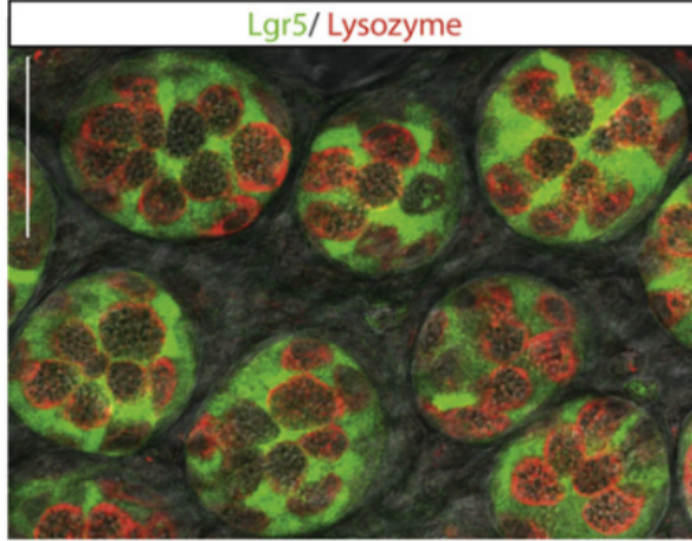
Figure 13: **Flourescent microscopy image of several crypt bases.** *Paneth cells have been stained for Lysozyme (red), stem cells for Lgr5 (green). From [19], Snippert et al., 2010.*

and a stem cell would correspond to the element λ_{12} or λ_{21}[7].

$$M = \begin{bmatrix} \lambda_{11} & \lambda_{12} & \lambda_{13} \\ \lambda_{21} & \lambda_{22} & \lambda_{23} \\ \lambda_{31} & \lambda_{32} & \lambda_{33} \end{bmatrix} = \begin{bmatrix} 0.3 & 1.5 & 1 \\ 1.5 & 0.3 & 1 \\ 1 & 1 & 1 \end{bmatrix} \tag{13}$$

In order to test the stability of this differential adhesion mechanism we chose to simulate the isolated crypt base as seen in Figure 14, gradually increasing time between stem cell divisions.

---

[7]Note that I am now actually allowing $\sum_i \lambda_i > 1$ or $\sum_i \lambda_i < 1$ and this now means that we are not guaranteed to have the same equilibrium distance between cells, i.e. 2 unit distances.
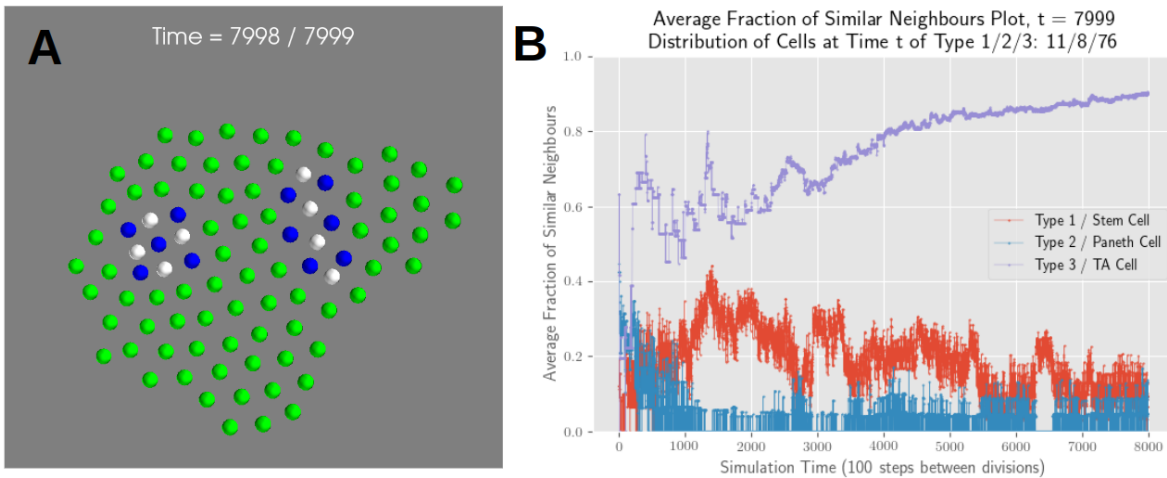
Figure 14: **Crypt pattern breaks apart, A, and stem cell neighbourhood shows clear fluctuations (red curve), B. 100 steps between divisions.** *Paneth cells (white), stem cells (blue) and TA cells (green). The patch of cells is initialized as a well-mixed salt and pepper pattern and then evolves according to the M-interactions. Stem cells divide every 100 steps. The crypt is seen to break apart into two smaller Paneth cell patches for stem cell divisions for divisions every 100 steps, i.e. for 80 cell divisions. The fractional neighbour plot, B, represents the average fraction of similar neighbours in the local neighbourhood for the three cell types. This was calculated and plotted as function of simulation time in order to estimate the stability of neighbourhood cell compositions. While the Paneth cells due to the M-interactions keep their local neighbourhood composition relatively constant, it is seen to fluctuate for the stem cells (red curve).*
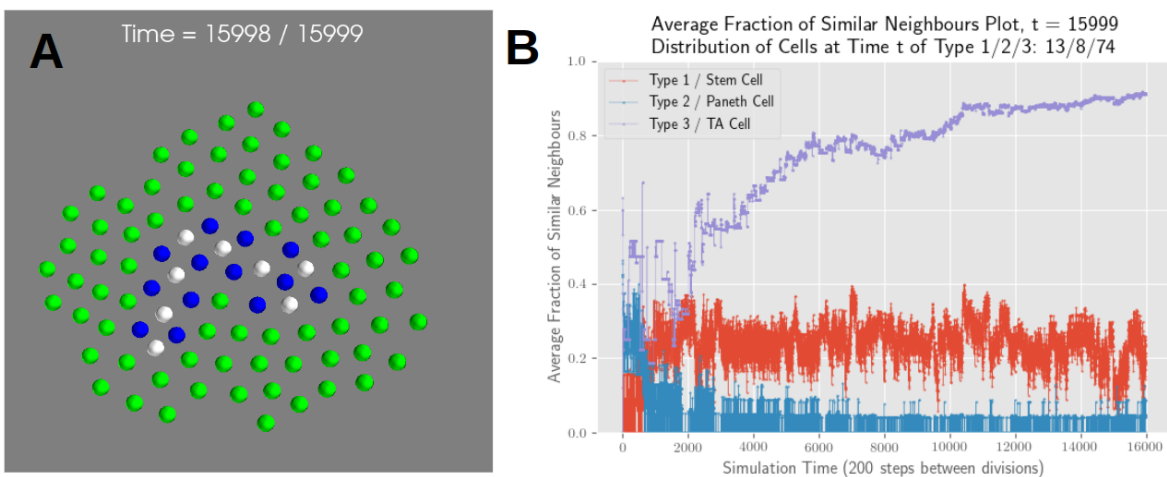
Figure 15: **Crypt pattern is stable. Fractional neighbour plot shows more stable neighbourhood for the stem cells. 200 steps between divisions.**

TA Cell Interactions				
Params	λ_1	λ_2	λ_3	λ_4
Value	0.7	0.25	0.07	0.2

Table 1: **Parameter values used to create Figure 9** Note that the TA cells are the subset of cells that interact through the S_4 mechanism, Eq. 12.

Paneth and Stem Cell Interactions				
Params	λ_1		λ_2	λ_3	λ_4
Value	$M[i_{type}, j_{type}]$		0.0	0.0	0.0

Table 2: **Parameter values used to create Figure 9**. M is the differential adhesion matrix which is only applied for Paneth cells and stem cells and their local neighbourhood.

When one increases the time between divisions, one notices less fluctuations for the stem cells. Further increasing the time between divisions to 200 steps yields a more stable crypt pattern as seen in Figure 15. In the above simulations, only stem cells divide and for a single stem cell at a time. *The stable pattern emerges if stem cells and Paneth cells have enough time to equilibrate after pushing out the new cell before a new one is added from divisions.*

The values chosen for M simply reflect a choice which seems to work well in ensuring proper mixing of the Paneth and stem cells. I find that this mechanism indeed is useful for producing a properly mixed state of Paneth cells and stem cells[8]. For investigations into the mixing of Paneth and stem cells, the efficiency of this dynamic for different stem cell division rates as well as how I specifically define the different cell types, see the Appendix.

Going back to how this mechanism relates to the first and second questions, I note that *the stability of the mixed pattern of stem cells and Paneth cells allow for an evenly distributed set of gradient vectors $\hat{G}_i$ that point radially away from the source of WNT3.* Differential adhesion and slow enough rate of stem cell divisions allow for the pattern to remain stable. However, even though some experimental data suggest that stem cell divisions alone are enough to account for the WNT3 gradient [18], I find that stem cell divisions and differential adhesion are not enough when used in combination to get a nice and circular swirling of PCP as illustrated in Figure 11. Because of this issue I need to run these mechanisms in parallel with cell-cell contact diffusion in order to have successful swirling of PCP vectors and subsequent budding of crypts. This will be clear from the next section.

---

[8]Animation of the mixing process from a small patch of cells (Paneth cells are white, stem cells are blue and TA cells are green) interacting through the M matrix with cell divisions every 500 steps at 2x playback speed: `https://www.youtube.com/watch?time_continue=507&v=slsh7uSqino&feature=emb_title`

2.1.3 Contact-Mediated Diffusion of WNT3

How does one ensure a more circular swirling of PCP vectors when divisions from stem cells alone are not enough to shape the gradient in the desired way? The authors of [4] mention that direct cell-cell contact also is responsible for the diffusion of WNT3. For this reason we choose to investigate if a mechanism capturing this direct cell-cell contact can help in ensuring more circular orientation of the PCP vectors due to the WNT3 gradient. In order to model the cell-cell contact mediated diffusion of WNT3 I chose to implement a gradient diffusion mechanism, Eq. 14. This is essentially a way to average the WNT3 gradient value over the local neighbourhood, i.e. over the Voronoi-neighbours, while taking the value of the cell for which the calculation is done into consideration as well.

$$w_i = \frac{w_i + \sum_j^n w_j}{1 + n} \tag{14}$$

with n being the number of Voronoi-neighbours of cell i and w_j the WNT3 gradient value of cell j. This mechanism relates to all three questions,

How does crypt shape emerge?
What determines the shape of the crypts?
How is shape maintained at high cell turnover?

Figures 16, 17 and 18 show how this mechanism helps in smoothening out the gradient which in turn improves the circular aligning of PCP vectors. If one does not take cell-cell contact diffusion of WNT3 into account one gets a WNT3 gradient profile that is clearly divided into distinct segments, as seen in Figure 16 **B**. For a detailed explanation of the assumptions and methods used for generating these plots, see the Appendix.

For Figure 16 **B**, I note that a WNT3 gradient profile of this nature is not able to induce crypt formation. However, when one includes the averaging mechanism, it is possible to have emergent crypt formation, as will be evident from the next section. It is clear from Figure 17 **B** that the WNT3 gradient profile rows from Figure 16 **B** have now been replaced by a more smooth distribution.

In reality, we do not know from experiment if the WNT3 gradient is distributed only from divisions, cell-cell contact or a combination of both. The results from this section, however, suggests to us that this mechanism not only acts as a sort of gradient correction mechanism but is also significant for establishing a WNT3 gradient which is capable of inducing emergent crypt budding.

The distribution can be smoothened even further, however, if instead we compute the contact diffusion at every division step instead of every other step, as shown in Figure

18 **B**, i.e. for every 200 steps, while also increasing system size. For this simulation, the initial configuration of the small patch of 16 cells has been embedded in a larger plane while also plotting the gradient $\hat{G}_i$ and PCP vectors for completeness.

Note in Figure 18 **A** the clear swirling of PCP vectors around the central Paneth cells. To summarize, there are two mechanisms at work that are the associated with a unique time scale; cell divisions and computation of passive cell-cell contact diffusion. Thus we have the ability to determine which mechanism is the most dominant. The timescales at which these mechanisms are computed determines which is the dominant mechanism for shaping the WNT3 gradient and I found that with single cell divisions every 200 steps and WNT3 cell-cell diffusion also every 200 steps I was able to get consistent crypt formation using the parameters shown in the Table 1 and Table 2. For investigations into the effect of increasing the time between computation of cell-cell contact diffusion, see the Appendix. For figures and details regarding tests carried out to induce crypt formation and budding, see Figure 35 (a) and (b) and the corresponding sections in the Appendix.

Going back to the questions posed in the introduction, this mechanism obviously relates to all three. *This is because the cell-cell diffusion mechanism helps in smoothening the gradient* which in turn yields more evenly distributed gradient vectors. This again makes the formation of a clear, circular swirling of PCP vectors easier. This is why it needs to be run alongside the stem cell divisions and differential adhesion, since one otherwise can have uneven and non-circular PCP swirls.

In the next section we will see that we are able to increase the gradient threshold and have crypt formation from a sphere under a new set of assumptions. This change in direction was decided after a meeting with the head of the BRIC group Kim Bak Jensen and BRIC researcher Hjalte List Larsen.
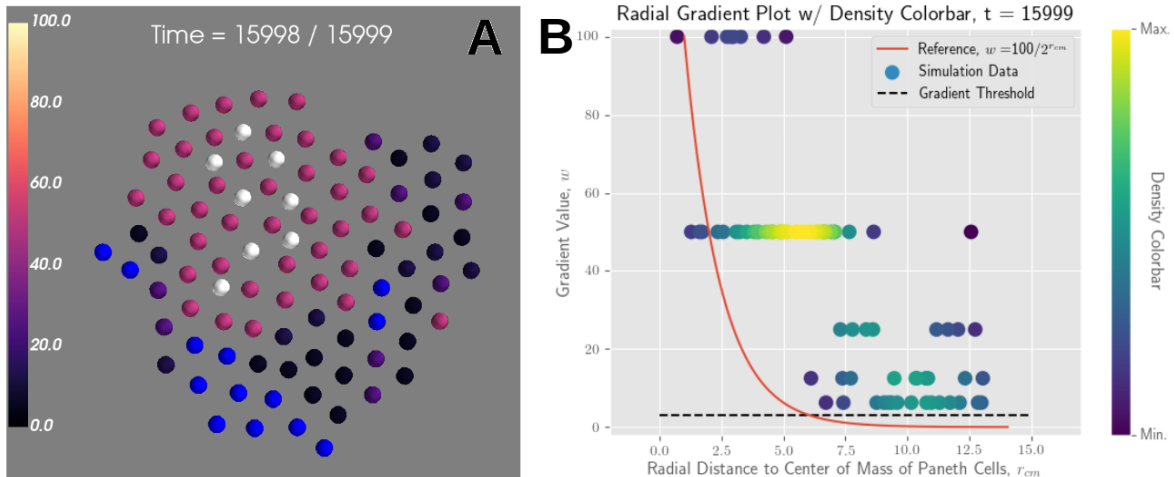
Figure 16: **Distribution of WNT3 gradient without contact diffusion is not smooth, A and B**. *Subfigure* **B**: *Paneth cells have gradient WNT3 value* $w_i = 100$ *and stem cells have* $w_i = 50$. *Upon stem cell divisions, the* w_i's *are halved for the two resulting cells. Also, a gradient threshold has been introduced that determines which cells interact through the WNT3 to PCP coupling mechanism. Furthermore, a reference function has been introduced (red curve in gradient distribution plot). This curve is an exponentially decreasing function and it reflects that we expect the WNT3 gradient distribution from cell divisions alone to be of a form comparable to this function, since we know that surface-bound WNT3 is halved upon stem cell divisions [4]. Note the two top rows on the gradient distribution plot on the right representing the Paneth cells and the stem cells. The distinct rows of cells reflect the fact that upon cell divisions the* w_i's *are halved. Other simulations initiated with different random seeds yielded similar outcomes. Blue cells have* w_i *below gradient threshold.*
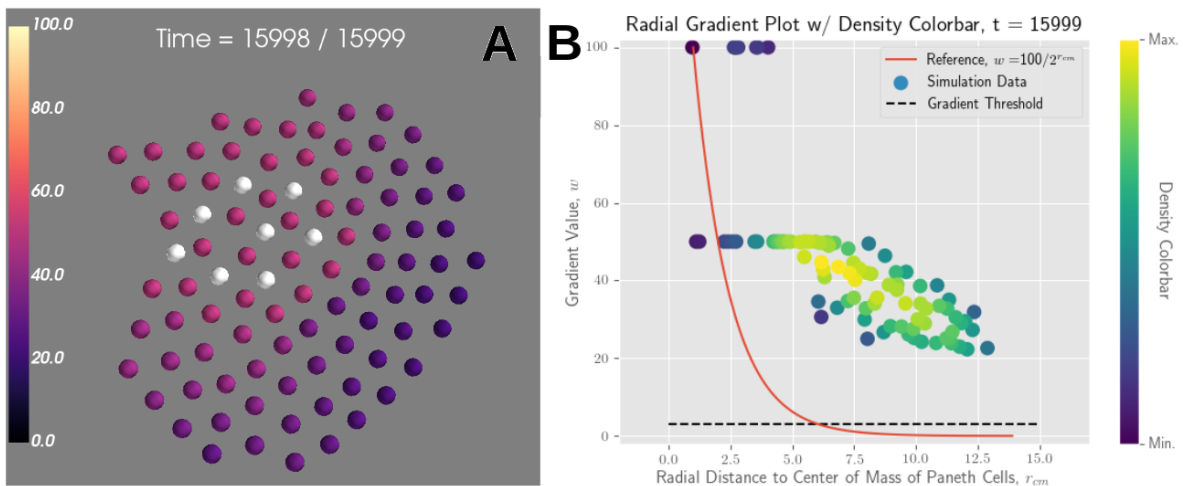
Figure 17: **Contact diffusion helps in smoothening the gradient**. *Distribution of WNT3 gradient from an initial patch of 16 cells (8 of them Paneth cells) after 16000 steps. Note how the WNT3 gradient distribution on the right is closer to the reference function while the color gradient is also more smooth on the left plot. Also, there are now no cells with* w_i's *below gradient threshold.*
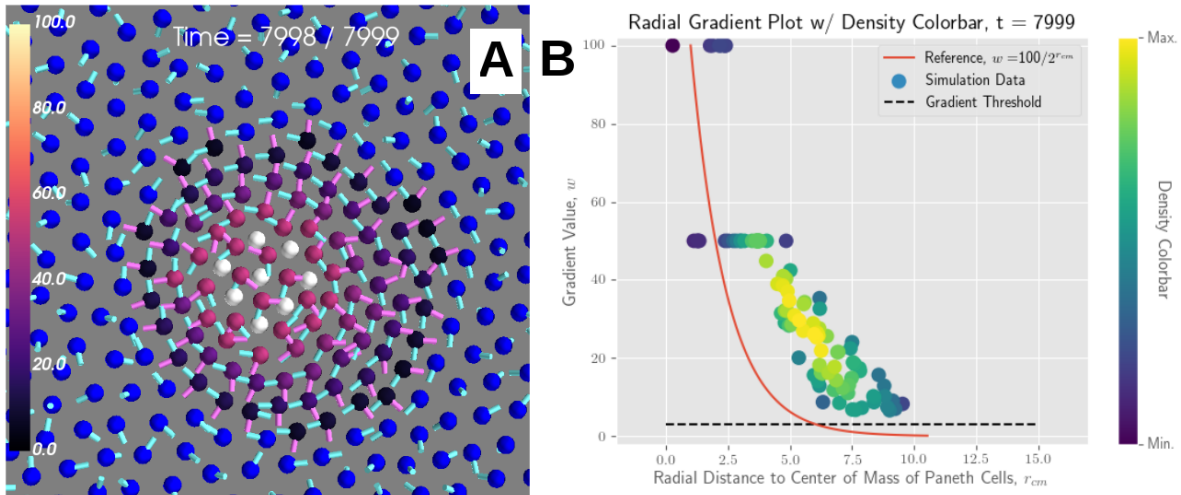
Figure 18: **Increasing rate of contact diffusion further smoothens the gradient**. *Distribution of WNT3 gradient from a plane of cells after 8000 steps. Gradient diffusion was calculated every division step, i.e. every 200 steps. Purple vectors represent the gradient vectors $\hat{G}_i$ and blue vectors are PCP vectors.*

2.1.4   Modelling Crypt Growth from Spherical Enterocysts

In the last sections I introduced the main mechanisms that were sufficient for crypt emergence. However, the results shown in the previous sections were obtained from simulations in the plane. After meeting with Kim and Hjalte from the BRIC group, we chose to go back to a more minimal version of the system more closely resembling intestinal organoid structures grown in the laboratory.

According to the BRIC group, *in-vivo* systems can grow crypts in the absence of Paneth cells[a] while in the case of organoids grown *in-vitro* crypt formation only occurs after the emergence of a Paneth cell.

---
[a]Paneth cells are not the sole sources of WNT, also the surrounding mesenchyme, i.e. the surrounding tissue, generate a WNT gradient.

Specifically, I now use the more realistic spherical enterocyst-like structures as initial configurations when running the simulations. Also, we look at the case of only one Paneth cell as opposed to a mixed patch of stem cells and Paneth cells. I thus embed a single Paneth cell in a spherical structure while using the same mechanisms as introduced in the previous sections in order to test if I am able to reproduce the growth of a crypt from a single Paneth cell.
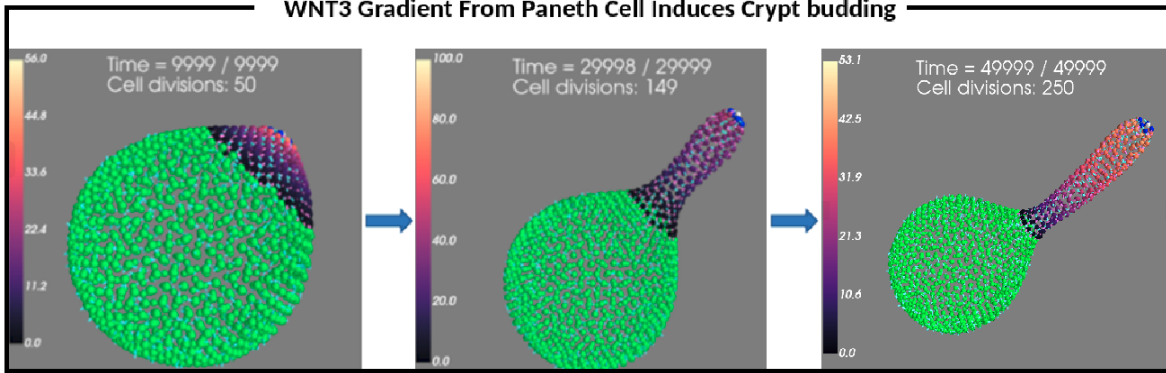
Figure 19: **Growing a crypt from spherical enterocyst comprised of 1000 cells**. *Simulation progress over 50.000 steps. Note how the protrusion has merely elongated while maintaining cell composition at the crypt tip when allowing for continued stem cell proliferation.*

Figure 19 shows a spherical configuration of cells with a protrusion from a single Paneth cell. For the simulations in Figure 19 the WNT3 gradient threshold has been increased[9], i.e. the gradient has not propagated to the rest of the structure as can otherwise be seen in Figure 9. Mostly the WTN3 gradient covers only the cells that were added to the system from stem cell divisions. The point of this section has been to show that emergent crypt formation is also possible with the model using a spherical system with only a single Paneth cell. I will now focus on explaining the possible experimental tests of the model.

2.1.4.1 Sending Model Predictions to BRIC for Experimental Tests What happens when the system is allowed to evolve (with and without cell divisions) under different assumptions for how PCP interactions are activated? Is there a feasable way to test which assumptions are most likely to be correct?

In order to test the stability of the emergent crypts we imagined that two mechanisms could be at play for determining PCP interactions, since little is known in the literature about how cells know when to orient themselves in specific directions.

- PCP could be inducible due to WNT3 in cells being above threshold,

  i.e. $w_i \geq w_{threshold}$

- PCP could be inherited from stem cell through divisions

The second idea is motivated by the authors in [20] describing an organizing region in

---

[9]Specifically, the gradient threshold $w_{threshold}$ was raised to $w_{threshold} = w_0/2^6$ from a previous value of $w_{threshold} = w_0/2^8$.

developing embryos which is comprised of a collection of cells that among other proteins also secrete WNT ligands. We imagine that one of these two scenarios could be how this organizing region works. Now, the choice of PCP orientation mechanism being based on either having WNT3 above gradient threshold or being based on cells inheriting PCP properties from stem cells yields four different possible scenarios as illustrated in Figure 20.

Figure 20: **Model predictions for morphological development of organoids based on whether PCP is inherited or induced. No stem cell divisions**. *Simulation started from spherical enterocyst-like structure embedded with a single Paneth cell. Time is reset for simulations **A**, **B**, **C** and **D**, so total simulation time is 80.000 steps. Same parameters as in Tables 1, 2.*

The reason for the 4 different outcomes in Figure 20 is that during the BRIC meeting, we were informed that two kinds of experimental tests were possible and did not require a lot of time and special equipment for preparing and treating the organoid samples. These consisted of checking the resulting morphological changes of the crypt-organoid structures grown in the laboratories (like the structure in Figure 2 and resembling the simulation in Figure 19) after subjecting them to two different tests:

1. The entire crypt-organoid structure is subjected to a uniform amount of WNT3 such that a high concentration of WNT3 proteins are available for all cells. This in our model corresponds to setting $w_i = w_0$ for all cells, i.e. $w_i = 100$.

2. The entire crypt-organoid structure is cleared of WNT3 such that no WNT3 proteins are available for any of the cells. This in our model corresponds to setting $w_i = 0$ for all cells.

26

The top row, Figure 20 **A** and **B**, represent PCP being inherited through stem cell divisions and thus PCP is only induced in TA cells since these are the resulting cells from divisions. For the bottom row, Figure 20 **C** and **D**, PCP is WNT3-inducible, i.e. cells that have $w_i \geq w_{threshold}$ interact through the entirety of Eq. 12 with parameters as given in Table 2. For the case **A**, the shape does not change over the course of 50000 steps and I conclude that the crypt is stable when the WNT3 concentration is increased to maximal value and PCP is inherited from stem cells. In the same column, case **C**, I note that the crypt-organoid system starts changing into a more tube-like structure. This is due to the fact that all cells have PCP interactions since all cells have $w_i \geq w_{threshold}$. Case **B** is seen to be stable when WNT3 is removed from the system and PCP is inherited from stem cells. In the bottom right, case **D**, the crypt-organoid system is seen to gradually revert back to the enterocyst-like state.
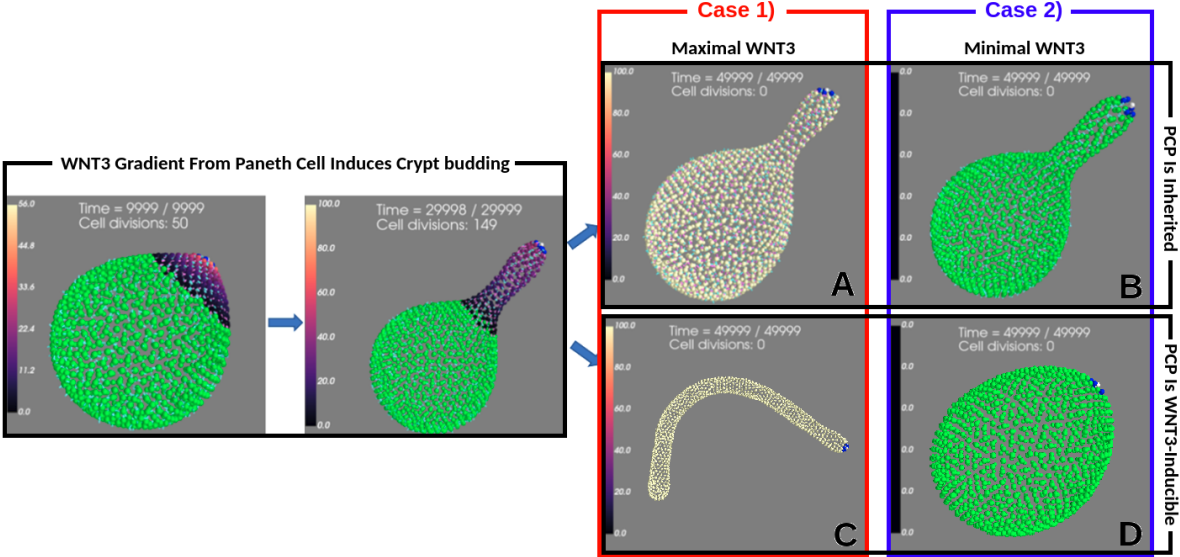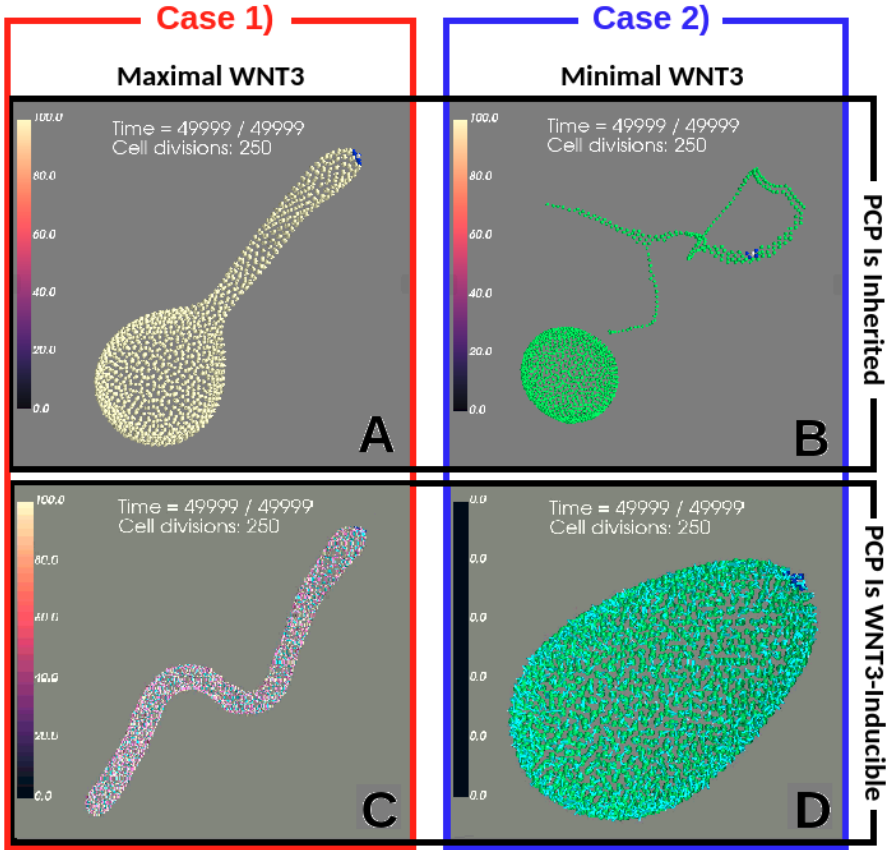

Figure 21: **Model predictions for morphological development of organoids based on whether PCP is inherited or induced. Now including stem cell divisions**. *Simulation started from spherical enterocyst-like structure embedded with a single Paneth cell. Same parameters as in Table 1, 2.*

The simulations in Figure 20 were all run for 50000 steps without cell divisions from the point of adding or removing WNT3 for simplicity. In order to check if the same trend is observed when stem cells are allowed to keep dividing I run simulations from the same

initial configuration but now with dividing stem cells. These results are illustrated in Figure 21. I note that the trend when allowing stem cells to proliferate is roughly the same, with the protrusion in case **A**, elongating as stem cells divide. Also, the tube transition is observed in in case **C** with the tube elongating with cell divisions. The transition back to the spherical enterocyst-like structure is again seen for case **D**. The system in case **B**, however, is seen to not be stable up to 50000 steps but breaks apart after roughly 2000 steps, so 32.000 steps in total. An interesting property also reported in [13] is the ability of the structures to self-organize and repair themselves. For case **B**, the protrusion breaks off but the main spherical structure stabilizes and repairs itself while the tip is growing more string-like.

In both test cases WNT3 is uniformly distributed, i.e. any pre-existing gradients vanish and thus all gradient vectors $\hat{G}_i$ are identically equal to zero. Now, $\hat{G}_i = 0$ means that I am unable to use directed division, as introduced in the Appendix. I thus choose a random direction for the newly added cells for these simulations. This means that all S_4-interactions in Eq. 12 are zero as well and thus absent. This again means that PCP vectors will not be oriented due to the local WNT3 gradient and thus the cells of interest have PCP interactions only through S_2 and S_3 in Eq. 12.

At the time of finishing writing this work the BRIC group had not yet responded with experimental results. We await their response with excitement!

2.2   Model Analysis

The set of working parameters in Tables 1 and 2 were initially chosen from the papers [13, 7, 11]. During work on the model, however, I changed these for other parameters that turned out to work well for the formation of crypts. In this section I will investigate in more detail the parameter regimes in which I see crypt formation and discuss the role of parameter values.

Specifically, we shall take a look at the parameters of the interactions in Eq. 12 that governs the motion through the inter-particle potentials, i.e. the values of $\lambda_1, \lambda_2, \lambda_3, \lambda_4$. I then relate simulation time to real time in order to compare crypt metrics obtained from simulation with experimental data. I then quantify crypt metrics, i.e. height, width, volume and number of cells in the crypts and then at the end focus on the parameters that control WNT3 gradient propagation and how this affects crypt formationh!

2.2.1   Parameter Sensitivity Analysis

The current working set of essential parameter values are as listed in Tables 1, 2, i.e.

TA Cell Interactions				
Params	λ_1	λ_2	λ_3	λ_4
Value	0.7	0.25	0.07	0.2

Paneth and Stem Cell Interactions				
Params	λ_1	λ_2	λ_3	λ_4
Value	$M[i_{type}, j_{type}]$	0.0	0.0	0.0

with

$$M = \begin{bmatrix} \lambda_{11} & \lambda_{12} & \lambda_{13} \\ \lambda_{21} & \lambda_{22} & \lambda_{23} \\ \lambda_{31} & \lambda_{32} & \lambda_{33} \end{bmatrix} = \begin{bmatrix} 0.3 & 1.5 & 1 \\ 1.5 & 0.3 & 1 \\ 1 & 1 & 1 \end{bmatrix} \tag{15}$$

I now investigate the parameter regimes in which we have crypt formation. This is done by a sensitivity analysis in which I use the current set of working parameters as a starting point. I then change one parameter at a time (OAT), while keeping the others constant, in increments of 0.05 from 0.05 to 1.0. We thus allow a maximal value of $\lambda_i = 1.0$ and a minimal value of $\lambda_i = 0.05$ for each parameter. We stop the search if at any point the crypts start to break apart or we do not have crypt formation. This then sets a parameter regime for each of the 4 parameters. Note that the parameters that are changed are those for the active subset of TA cells (for these investigations chosen as those cells that have w_i above gradient threshold) and as such, we are not interested in changing the values of the M-matrix[10].

2.2.1.1 Parameter Scan Naively, the above considerations mean that each parameter has a maximum of 20 values, which for 4 parameters gives a maximal parameter space of size $20^4 = 160000$ if all combinations were to be explored. However, this was much too time consuming and my approach instead explores 80 combinations, 20 for each parameter with the other parameters constant. Each case is run for 30000 steps with stem cell divisions every 200 steps to replicate the conditions that lead to the crypt that formed the basis for the predictions generated for the BRIC team, Fig. 20.

I thus define a crypt as stable if it is still intact at the end of the simulation.

Value	0.05	0.10	0.15	0.20	0.25	0.30	0.35	0.40	0.45	0.50
λ_1	✗	(✔)	(✔)	(✔)	(✔)	(✔)	(✔)	(✔)	✔	(✔)
λ_2	✗	✔	✔	✔	✔	✔	(✔)	(✔)	(✔)	(✔)
λ_3	✔	(✔)	✗	✗	✗	✗	✗	✗	✗	✗
λ_4	✔	✔	✔	✔	✔	✔	✔	✔	✔	✔

---

[10]Since we are now also working with only 1 Paneth cell we believe that the effects from having the pairwise attraction greater than 1 for this small subset of cells has negligible effect on the overall formation of crypts. However, this may be wrong to assume and will be discussed in Section 4

Value	0.55	0.60	0.65	0.70	0.75	0.80	0.85	0.90	0.95	1.00
λ_1	(✓)	✓	✓	✓	✓	✓	✓	✓	✗	✗
λ_2	(✓)	(✓)	(✓)	(✓)	(✓)	✗	(✓)	(✓)	✗	(✓)
λ_3	✗	✗	✗	✗	✗	✗	✗	✗	✗	✗
λ_4	✓	✓	✓	✓	✓	✓	✓	✓	✓	✓

Table 3: **Parameter sensitivity analysis from working set of parameters. The analysis reveals certain regimes for which crypts emerge.** *A checkmark corresponds to successful crypt formation whereas a cross means the crypt never formed. A checkmark in parenthesis means that a crypt was formed, but broke apart during the simulation. For each cell in the scheme, only that parameter was varied and the rest kept fixed as per the baseline set of parameter values Tables 1, 2. The random seed used to run the simulations was set to 42.*

For the first parameter λ_1, the crypts that form from 0.10 and on are small at first and then grow larger as they get more stable with time for higher parameter values. In general, the crypts for low λ_1 are very unstable since the adhesion is very weak, which is also reflected by the fact that the inter-particle spacing is very large compared to the crypts that form from higher values of λ_1. At $\lambda_1 = 0.95$ the tendency to remain spherical dominates over crypt formation and the crypt protrusions are very wide and very short. For the parameter λ_2, crypts again start out small but then grows longer and narrower as the parameter is increased. After $\lambda_2 = 0.30$ the crypts start to break apart and get smaller again, though. For λ_3, our parameter scan supports the findings that the authors in [13, 7, 11] also report, namely that the range of viable parameter values is very narrow. For higher values, the crypt breaks apart very early on in the simulations. For λ_4, the lower values produce very wide crypts and as the value is increased, the crypts become increasingly narrower and longer. At roughly 0.55 and above, the crypts begin to grow shorter and wider again, qualitatively not resembling crypt protrusions as e.g. shown in [18].

To sum up, the range of parameters yielding stable crypt formation from OAT sensitivity analysis are, when excluding some points in between the ranges that fail, e.g. $\lambda_1 = 0.50, 0.55,$

$$\lambda_1 \in [0.45; 0.90]$$
$$\lambda_2 \in [0.10; 0.30]$$
$$\lambda_3 \in [0.05; 0.10]$$
$$\lambda_4 \in [0.05; 1.00]$$

The same entire parameter scan was redone with 3 other random seeds to see if the parameter regimes changed dramatically. For the tables corresponding to these parameter scans see the Appendix. I note that the overall behaviour is the same with minor variations.

2.2.2 Statistics and Analysis of Crypt Metrics

How do the investigated parameters affect crypt number of cells, crypt height, diameter and volume? This section introduces the results obtained from analysing the data generated from the parameter sensitivity analyses. Specifically, I measure number of cells of the crypts, crypt height, diameter and volume and compare the first three of these to in-vivo experimental data from mice, since these quantities have been measured and reported in [2]. Finally, I briefly report how varying the time between computing the WNT3 gradient propagation from cell-cell contact diffusion affects crypt formation. For explanation of the methods used, as always see the Appendix.

2.2.2.1 Crypt Growth Efficiency For the above 80 combinations of parameters, I have stable crypt formation in 34 cases which is equivalent to a crypt formation efficiency of 43%. The authors of [18] report a maximum efficiency rate of successfully grown laboratory organoids of 18% for Lgr5 stem cells. When computing the average successful growth rate from the other parameter scans the growth efficiency is 42% when grown from the working set of parameters. It is obvious that these numbers are not directly comparable since I am modelling crypt growth from an already formed enterocyst-like structure. Nonetheless it sheds some light on the fact that a certain set of parameter values are needed for successful crypt formation.

2.2.2.2 Relating Simulation Time with Real Time In order to relate simulation time with real time we use the stem cell cycles, i.e. the time between successive stem cell divisions from the same cells, since these are reported in the literature. The stem cell cycles from simulations were determined by computing and saving for each simulation the number of steps between divisions from the same cells, i.e. the stem cell cycles. I then plotted these distribution of these as in Figure 22 and from these computed the mean of each distribution. These were then combined using an averagefor a final estimation, relation 16, with the error equal to the sample standard deviation.

A collective average was then calculated with the error corresponding to 1 standard deviation. An example of two distributions for different random seeds is shown in Figure 22. For all simulations, stem cells were again chosen every 200 steps for division. Running 6 simulations with different random seeds and computing the above distributions for each yield a final estimate for the stem cell cycle

$$\text{cell cycle} = 2092 \pm 73 \text{ steps} \tag{16}$$

The authors of [14] report a stem cell cycle of roughly 24 hours, whereas the authors of [19] report a *stem cell replacement rate* (which is to be understood as the same as the stem cell cycle) of 0.74 ± 0.04 per 24 hours, corresponding to a cell cycle of about 32 hours. This is also what is reported in [14] as the upper limit, since in this paper the authors note that stem cell cycles show great variance and is measured as low as
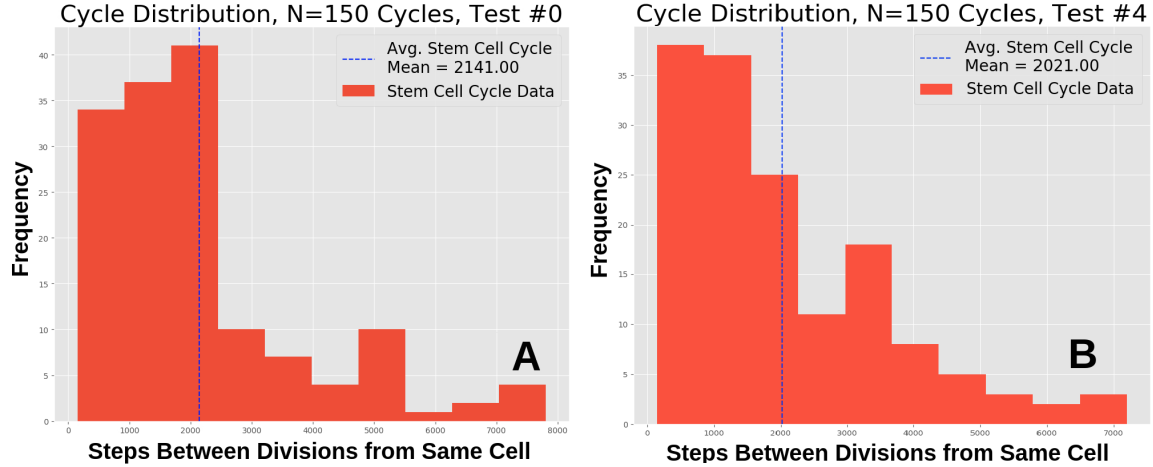
Figure 22: **Distributions of stem cell cycles from 2 different simulations.** *Histogram* **A** *has mean cycle 2141 steps and* **B** *has mean cycle 2021 steps. As also reported in the literature, I find that the stem cell cycles are spread out and not uniform.*

12 hours. The authors of the seminal paper[11] [15] report a stem cell cycle of 12 hours. We choose to use this estimate on the cell cycles together with our result (16) since this paper explicitly deals with an in-vitro organoid system and not in-vivo gut structures. Combining these data, we get a correspondance between simulation time and real time such that

$$1 \text{ simulation step} \approx 0.006 \text{ hours} = 21 \text{ seconds} \tag{17}$$

Using this as the working correspondence we then have that all simulations up to 30.000 steps, i.e. the simulations used to compute crypt metrics, correspond to a real time growth time of about 7 days starting from the spherical enterocyst-like structure. From a numerical aspect, simulation data is only saved every third step in order to save space, so 1 simulation step corresponds to 3 steps of $dt = 0.1$. This again relates simulation time step dt with real time such that $dt = 7$ seconds in real time.

2.2.2.3   Number of Crypt Cells, Crypt Height and Diameter   The crypts that were successfully simulated in the parameter analysis were then subsequently filtered out from the data, analyzed and the metrics computed and plotted as function of parameters $\lambda_1, \lambda_2, \lambda_3, \lambda_4$. In this section I report the number of crypt cells, height and diameter for combined data from all 4 random seed tests.

---

[11]Sato et al., 2009, for the first time demonstrate how they can successfully grow self-organizing intestinal organoids from single Lgr5 stem cells in the absence of a mesenchymal niche.
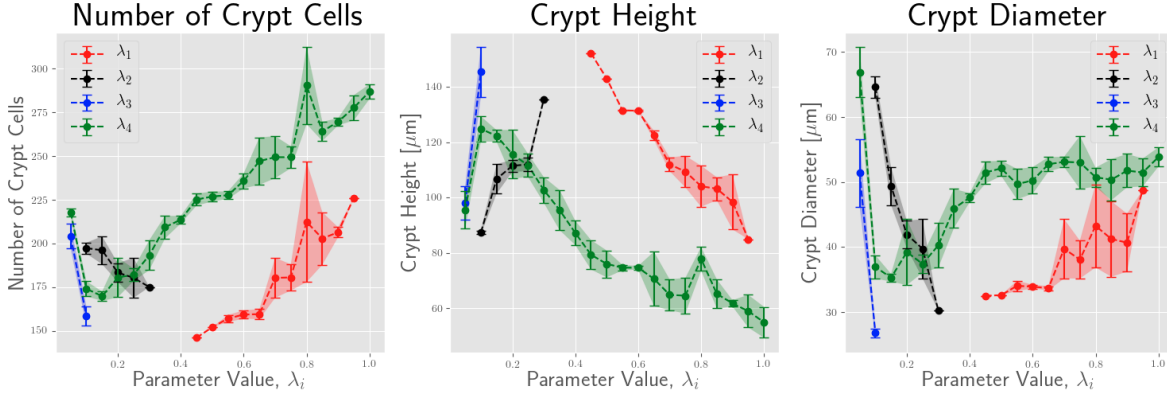
Figure 23: **Crypt metrics show clear, common trends when changing model parameters governing polarity-based attraction and repulsion.** *Metrics captured at end of simulations, i.e. at 30.000 steps or roughly 7 days. If instead we use the higher estimate for stem cell cycles, growth time is roughly 19 days. It is worth to note that I seem to capture the same behaviour of decreasing tube diameter when increasing λ_3, as also reported in [13, 7, 11]. However, more data would be needed in this regime to establish this firmly since I am only allowing parameter values to vary in increments of 0.05. Furthermore, increasing λ_1 has the intuitive effect of shortening the crypt heights, which makes sense when remembering that stronger λ_1-interactions favor more spherical structures. The tendency for crypts to grow shorter and wider when increasing λ_4 is also observed. The data points are sample averages over all random seeds used with errorbars equal to 1 sample standard deviation. Very small errorbars are due to the fact that only one data point was obtained for that sample for that particular parameter value. This means that only one of the 4 simulations using different random seeds yielded successful crypt formation. As such, a maximum of 4 values go into each data point. Some data points may however also just be very close to each other.*
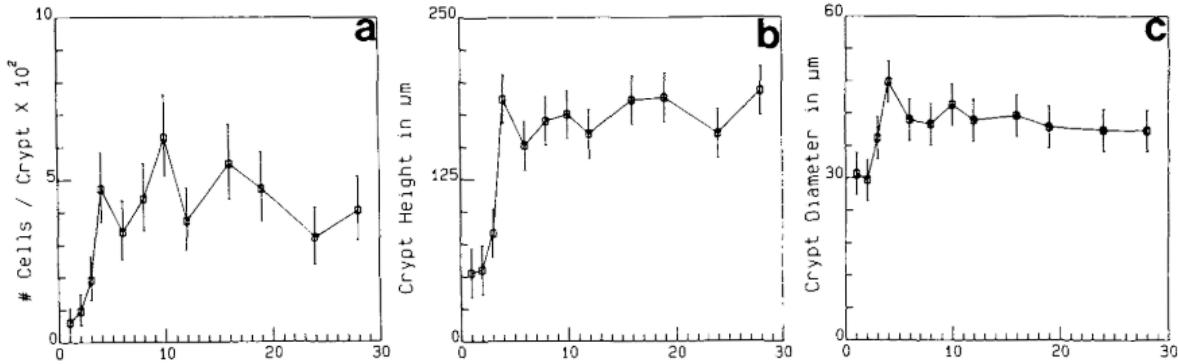

Figure 24: **Crypt metrics as function of age.** *From [2], Cheng et al., 1985. The authors report that after about 4 weeks the measured number of cells stabilize at a level of 450 cells per crypt. The same is true for height and diameter of the crypts, where the height stabilizes at roughly 170 µm and the diameter at about 40 µm.*

Comparing **crypt number of cells** from simulations with experimental data, *the experimental data suggests to me that we should allow the simulations to run for at least twice as long if we want a level matching the 4 week-mark*, since number of crypt cells are below 250 cells for all parameters.

Crypt heights from simulations seem to vary around 100 μm and *running simulations longer would in my mind most likely yield greater crypt heights from simulations, thus more closely resembling experimental data. This is because crypts tend to elongate with stem cell divisions.*

Crypt diameter seem to vary around the reported value of 40 μm, but this metric also does not display the same change over time as the number of crypt cells and crypt height as reported by the authors of [2]. *One can also interpret the results as more closely matching the 3-week diameter, since here the cells per crypt are reported to be around 200.* This would also better match the range of crypt heights, but would in turn mean that *our estimate for stem cell cycle should be associated with the upper limit of roughly 32 hours* as reported in [14, 19] as opposed to 12 hours. If we choose instead 32 hours as the stem cell cycle a simulation time of 30.000 steps would then correspond to about 3 weeks of growth time. This better matches the number of cells and crypt heights as well as not being very far from the reported widths.

For plots capturing the crypt volume 44 in the Appendix. For a discussion relating to the comparison of in-silico simulation data with in-vivo data, see the Appendix. The length scale for describing crypt metrics was determined by reviewing the images of intestinal organoid glands and the cells composing them as well as the associated scale bars in [15]. From the images I inferred a scale of 5 μm for the radius of an intestinal crypt cell. Using this scale, the inter-particle equilibrium distance is thus equivalent to 10 μm.

2.2.2.4 WNT3 Gradient Propagation We know from the article [3] that the mechanism most likely responsible for establishing the WNT3 gradient is division from stem cells. As such, I thought it worthwhile to investigate if I could still have crypt formation if I increased the time between contact mediated diffusion of the WNT3 signal, since the results obtained so far have been obtained using 200 steps between contact mediated diffusion as well as cell divisions, i.e. the two mechanisms operate on the same time scale. I find that it is indeed possible to have successful crypt formation at $t = 30.000$ steps for up to 800 steps between contact-mediated diffusion. Using more than 800 steps between contact diffusion, I find that the crypts tend to grow small and very wide, resembling the effect of using a high value of λ_4.

For figures showing crypts as well as WNT3 gradient distributions see the Appendix.

3 Discussion and Conclusion

In this work I set out to try and answer the questions posed in the introduction,

How does crypt shape emerge?
What determines the shape of the crypts?
How is shape maintained at high cell turnover?

through the addition of new dynamics to the original model [13]. In this section I first summarize the main results obtained during this work and conclude with the applicability of the model and findings. I look at where the model has its pitfalls and room for improvements and I end the section with a discussion of the assumptions and methods used as well as ideas for further work with the model.

3.1 Main Results and Conclusions

> *The main hypothesis of this work is that a gradient of WNT3 which emanates from the WNT3-secreting Paneth cells acts as an organizing signal so as to orient PCP in the transit amplifying (TA) zone to induce crypt formation.*

Eqs. 10, 11 and 12, i.e. the WNT3 to PCP coupling, represent the main results of this work together with differential adhesion[12], Eq. 13 and WNT3 cell-cell contact diffusion, Eq. 14. Furthermore, apical-basal constriction is introduced in the Appendix and turns out to be beneficial in crypt budding for high values λ_1, since otherwise the cell plane stays flat. *These mechanisms together are sufficient and necessary for emergent, stable growth of intestinal crypts under the main hypothesis. These crypts, as investigated from OAT parameter sensitivity analysis, are able to maintain cell composition at the crypt tip during stem cell proliferation and are stable*, i.e. not breaking apart, up until a growth time equivalent to 19 days using the highest estimate for stem cell cycles. If one uses the low estimate, then this growth time is instead 7 days. Some of these crypts will persist for even longer and merely elongate. *The results from WNT3 diffusion by cell-cell contact suggests to us that perhaps this is a significant mechanism in ensuring proper alignment of PCP.* The main quantitative results for crypt metrics, i.e. the parameter regimes and the parameter values' effect on metrics in Figure 23, show clear, common trends, e.g. crypts becoming shorter when increasing λ_1 and λ_4. I also rediscover the tendency in [13, 7, 11] for crypt diameter to decrease when increasing λ_3, which also has a very narrow range for emergent, stable crypt formation. *When comparing results from parameter analysis to experimental data, I find that crypt metrics resemble the ones reported for 3 week old laboratory mice. Specifically, diameter seems to vary close to the results reported in [2], about 40 μm.*

---

[12]The salt and pepper pattern, however, could in principle also have been modelled using a greater level of noise in the equations of motion if this noise was allowed to vary between cells, as I was made aware by PhD student Alexander V. Nielsen.

These results tell us, under the main hypothesis, that crypt shape emerges and is determined by the orientation of PCP due to a local gradient of WNT3, which acts as an organizing signal, as well as by the specific strengths of the individual polarity interactions, i.e. λ_1, λ_2, λ_3, λ_4. Crypt shape, especially the salt and pepper pattern, is maintained through differential adhesion and WNT3 cell-cell contact diffusion.

How can the model be applied? One idea is what has been described in the main text and discussed with the BRIC group, where the assumptions underlying PCP activation, i.e. if PCP is inherited from stem cells or activated due to a certain concentration of WNT3 on the membranes, can be tested experimentally by observing the resulting organoid shapes from these tests. If PCP seems to be activated due to WNT3 levels, then the threshold parameter could yield information about this threshold in real life, if one such exists. Furthermore, these results in principle allow for the fine-tuning of parameters. However, this is fine-tuning for one parameter at a time only, keeping the others constant. If I change all four parameters at the same time to the most optimal values most closely resembling data [2] and run a new set of simulations, the crypts are not stable. One might, if a truly optimal parameter set can be estimated such that crypt metrics from simulation better match experiment, use the found restrictions on the parameters in future work to shed light on the microscopic interactions that truly govern these behaviours. For example, an idea is that the strength of polarity interactions correlate with concentrations of different regulatory proteins involved in AB or PCP pathways. This obviously would require more work and closer cooperation with experiments and is not in the scope of this work.

What are the pitfalls? An obvious lack of the model is the ability for cells to undergo mitosis, i.e. to die and be removed from the system. In real life, the emerging gut structures are stable under constant cell renewal. This means there is both a source and a sink for cells in the system. If one could implement cell death at the crypt tip as discussed in later sections one might be able to achieve a more accurate model. Such a model could perhaps yield stable crypt metrics as the ones that stabilize after the 4 week mark in [2]. Following [13], one could also have included pressure from the surrounding growth medium in order to investigate crypt emergence under different circumstances.

3.2 Assumptions and Methods

3.2.1 Modelling Cells as Point Particles

One obvious simplification of the work is the treatment of single cells as point particles. This, however, constitutes a very deliberate choice of the original authors of [13] since this greatly reduces the complexity of the modelled system that otherwise would require a great deal more subsystems of signalling pathways, models of cellular mechanics, etc. Furthermore, given that we are able to get emergent, stable crypt formation from a simple set of interactions, this stresses the point that most likely one does not need to simulate all of the microscopic interactions. Instead, we can use macroscopic approximations of AB and PCP polarities as well as the WNT3 gradients represented as vectors and still capture the overall morphology.

3.2.2 Determining Cell Stemness

Another set of assumptions used are those that govern how I determine what cells are stem cells in the simulations. I thought of and implemented a few key properties of stem cells, such as cell plasticity. Cell plasticity is the possibility of a stem cell becoming a TA-cell and vice versa in the absence or presence of Paneth and stem cells in the local cell neighbourhood. I did not choose to go forward with the idea of defining stem cells based on the local concentration of WNT3, since this in our opinion was not well documented in the literature. Also, this method proved very sensitive to small changes in WNT3 concentration and as such proved difficult to use since cells would, for example, cycle in between differentiated states and not provide a stable cell division output.

3.2.3 Parameter Sensitivity Analysis

The OAT parameter sensitivity analysis used in this work was chosen due to its simple implementation and prevalent use in the literature. Though it is simple, it gives an idea and overview of how varying one parameter changes the metrics as function of that particular parameter value. However, it does have its pitfalls. For instance, since the OAT analysis does not take into account variance and correlations, e.g. how changing 2 parameters at the same time changes the behaviour, it does not capture the more complex nature of the interactions. This was especially evident when I tried to change all the working parameters to the ones obtained from OAT analysis that best matched experimental data. Using these "optimal" parameters I then found that the emerging crypts were not stable up to 30.000 steps but instead broke apart less than halfway through the simulations, i.e. the obtained parameter values from OAT analysis did not work well when combined. This again speaks to the complexity of the interactions and how it is difficult to estimate the best set of parameters, at least if stability is of importance. Finding optimal parameters is also difficult owing to the fact that the requirement we use for determining whether or not a parameter is viable is whether or not we have successful crypt formation - which at the time of finishing this

work was done by visually inspecting each single result from simulations. An obvious improvement to the work would thus be to write an algorithm that can tell you, as the simulation progresses, if a crypt has broken apart or is still intact. From this, one could then automate the parameter search even more and based on this information on crypt stability then perhaps even make the parameter search of the kind that takes into account variance and correlations between parameters. Finally, it is also worth mentioning why I did not choose to make the parameter scan for also the parameters of the M-matrix. First of all, M affects only a very small subset of cells. Secondly, the parameters were seen to give the desired results of mixed stem cell and Paneth cell patterns, i.e. resembling the patterns shown in Figures 1 and 13. One could argue that the values chosen for the parameters might affect the rate of successful crypt formation. This might very well be true. However, I saw that lowering the values resulted in less well mixed cell patches and an increase in the inter-particle equil. distance.

3.2.4 Comparing Results for In-Silico Growth with In-Vivo Data

The results obtained are compared to experimental data from mice dating back to 1985, since it has proven difficult for me to find in the newer literature measurements of these kinds. I attribute this to the fact that the field has progressed a lot since then, putting less emphasis on and need for measurements of macroscopic quantities like crypt height, diameter, etc, and more emphasis on the details of the numerous microscopic interactions involved in e.g. signalling pathways which is much more accessible nowadays through e.g. flourescent microscopy techniques. The fact that I compare in-silico data to experimental in-vivo data could be questioned as not feasible, but since organoid cultures increasingly display behaviours and properties also reported for in-vivo gut systems [9, 10, 18] I have decided to do it this way.

3.3 Model Observations and Ideas for Further Work

3.3.1 Crypt-Villus System as Shown in Figure 33

While working developing and testing the intestinal organoid model using an externally fixed, exponentially decreasing gradient to model the WNT3 signal spreading due to cell divisions, I encountered the result shown in Figure 33 in the Appendix. This constitutes a very interesting and extremely rare result from an older version of the model in which what looks like both a crypt and a villus forms. This was observed only once. There are several aspects of this result that are worth noting. First of all, the result was obtained in a plane for a global gradient, i.e. as shown in the figures, the whole plane adjusts it's PCP vectors such as to have a central point about which all vectors orient themselves. This is in opposition to what is done later in the model, where only a certain fraction of cells are allowed to adjust their PCP vectors based on the WNT3 gradient. Global gradients have parallels to the in-vivo intestinal system, where the surrounding mesenchymal cells also generate a WNT signal. However, the authors of [15] show that the formation of crypts in organoids do not require the mesenchymal

niche, *but as far as I can tell they do not report if this is also true for villi.* In the figures, it is also worth noting that the villus is longer than the crypt, which is also true for in-vivo systems. However, when letting the system evolve even further, the crypt and villus break apart and as such, the system is not stable. For future work, investigating this system more in-depth could be very interesting.

3.3.2 Self-Organization and Self-Healing

As in the original paper [13] I also find that the structures are able to at least partly self-organize and heal in the case of crypt failure, i.e. if the crypts break apart and the simulation is allowed to continue. The direct parallel here is of course in wound healing and epithelial self-repair. Figure 25 shows an example of such a crypt failure and subsequent self-healing and self-organization of the main structure.
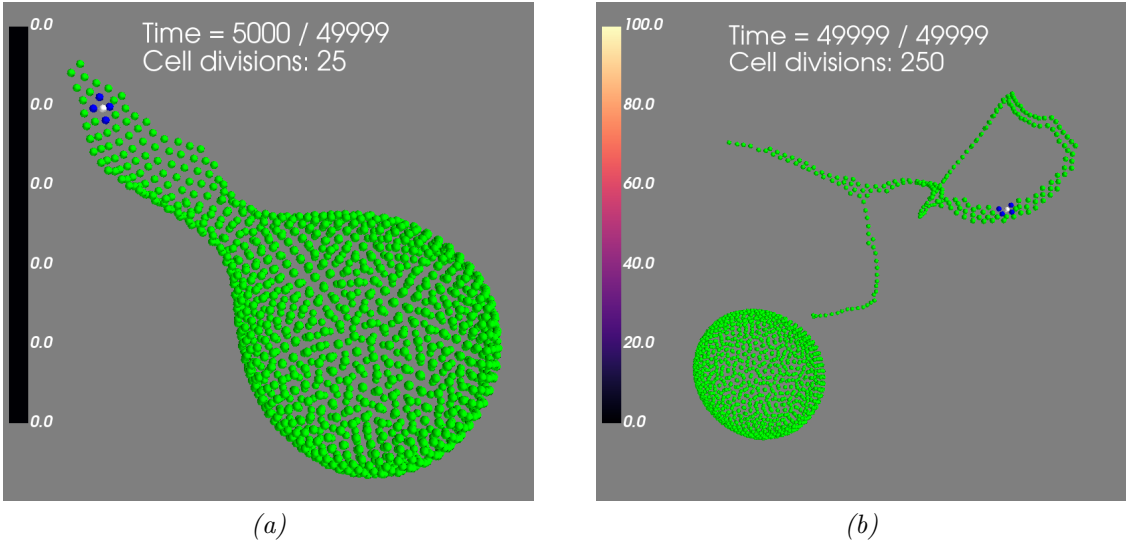

(a) (b)

Figure 25: **Structure partly self-repairs after crypt breaks apart.** *Subfigure a) Crypt breaks apart and Paneth cell compartment breaks off. Subfigure b) Spherical enterocyst-structure self-organizes and heals while the tip that broke off grows more string-like with divisions*

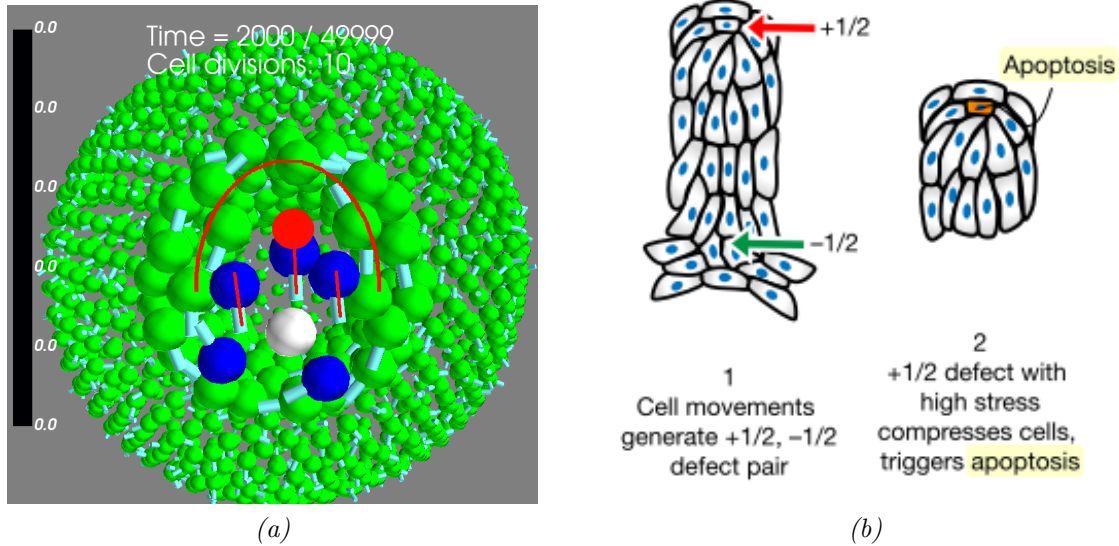39

3.3.3 Topological Defects Observed in Failed Crypts

Figure 26: **a) "+1/2" topological defect is observed prior to crypt breaking apart. b) Formation of a topological "+1/2" defect precedes apoptosis.** *From [16], T. Saw et al., 2017. 1b) not to be confused with an actual crypt. For subfigure a), the great red dot represents the point of the nematic defect. Note also that for a), this simulation was run while making predictions for the BRIC group, case **B**, Figure 21. As such, there is no WNT3 gradient because $w_i = 0$ for all cells.*

During model simulations, I have seen in multiple of the failed crypts that a certain pattern precedes the breaking apart of the crypt tip. Namely, the formation of a "+1/2" topological defect as illustrated in Figure 26. The same pattern can be seen preceding apoptosis in the paper [16]. The defects tend to come in pairs[13] The fact that these defects are known to precede apoptosis and the fact that I see these at the closed tip of elongated tubes, i.e. the crypt bases, together with the knowledge that at the tip of the villi, cells are undergoing apoptosis suggest to me that perhaps apoptosis at the villus tip is governed by the same mechanism or a mechanism closely related to this. Of course, this need not be the case but I find it very interesting nonetheless, and perhaps this could be used moving forward in a model with villi implemented as well to determine the site of apoptosis. The fact that the nematic defects also arise in pairs in the simulations to me are very interesting and is yet an interesting parallel to in-vitro cell experiments [16].

---

[13]See Figure 31. Here, the central +1 nematic defect accounts for the two -1/2 defects on either side of the central bulge. This pattern is seen in numerous simulations during the work.

3.3.4   Ideas for Including Crypt Fission

As mentioned briefly in the introduction, crypts grown both from in-vivo and in-vitro samples show the ability to sort of melt together in a process known as crypt fusion. Crypts can also go the opposite direction and split into two in a process known as crypt fission. These processes are not completely understood, but studies have shown that crypt fission is probably initiated when Paneth cell-rich regions are separated by small clusters of Lgr5 stem cells [9].

In Figure 38, as in the main text, two Paneth-cell rich regions are separated, although TA cells are in between them. This sort of resembles what the authors of [9] describe as a precurser for crypt fission. One could easily imagine that if one has a stable crypt, stem cells could be put to divide more rapidly and thus create an environment at the crypt "tip" in which the salt and pepper pattern of stem cells and Paneth cells break apart. This could perhaps then result in a similar pattern at the crypt tip and result in emergent crypt fission. I note that I have added the functionality of divisions from Paneth cells to the model, but further work has not been done to investigate if I can recreate this phenomena.

3.3.5   Ideas for Further Investigations into Morphological Dynamics

How do the simulated crypts evolve over time? It is in principle doable from the data at hand to compute the time evolution of the crypt metrics such as number of crypt cells, height and diameter. Doing so would yield deeper insight into the temporal evolution of the system and at the same time make possible a direct comparison of crypt metrics as function of time as is also reported for laboratory mice in [2].

4 Appendix

4.1 Intestinal Organoid Model

Before the model developed in this work reached its final and current form I worked on a variety of approaches, using a variety of assumptions first for plane geometries and then for spherical geometries, the latter much more closely resembling the intestinal organoid structures observed in experiments. This section shows the chronological order in which the different approaches were examined and how to model came to be in its current form.

4.1.1 Modelling the Intestinal Crypt

In order to get the PCP vectors of the cells of interest to swirl around the Paneth cell(s) and hopefully lead to convergent extension (CE, a type of cell movement where the cells move e.g. along the crypt axis instead of widening the crypt) and crypt formation, I needed a mechanism to orient the PCP vectors. To this end, I implemented a mechanism first for nearest neighbours of the Paneth cell(s) only, before the introduction of a WNT3 gradient. I then implemented divisions from stem cells and looked at PCP inheritance for the experimental tests for the BRIC group. This means that only cells that are the direct offspring of stem cells inherit the property of non-zero PCP interactions and the rest of the cells in the simulations only interact through the AB vectors, meaning $\lambda_1 = 1$ for cells with no PCP inheritance and all other interactions equal to zero.

In the following sections, the entire plane or sphere is initialized with only $\lambda_1 = 1$, rest equal to zero. Thus, only the cells of interest and/or their nearest neighbours have interactions with $\lambda_2, \lambda_3, \lambda_4 > 0$.

4.1.1.1 Orienting PCP for Nearest Neighbours of Paneth Cell
To explicitly model the dynamics of the Paneth cells inducing PCP changes in its neighbours, I first started by initializing a plane with a single Paneth cell. This Paneth cell then induces PCP changes in its nearest neighbours only, modelled through a new term $\lambda_4 S_4$ which was added to Eq. 1, thereby introducing 1 new parameter to the model. Again, λ_4 is a scalar and S_4 is a cross product:

$$S = \lambda_1 S_1 + \lambda_2 |S_2| + \lambda_3 |S_3| + \lambda_4 S_4 \tag{18}$$

$$S_4 = (\hat{q}_i \times \hat{r}_{ij}) \cdot (\hat{q}_i \times \hat{r}_{ij}) = 1 - (\hat{q}_i \cdot \hat{r}_{ij})^2. \tag{19}$$

Eq. 19 has the effect through the potential interactions of trying to make the PCP vectors of the nearest neighbours to the Paneth cell orthogonal to the distance vector between them, i.e. $\hat{q}_i \perp \hat{r}_{ij}$. This is sufficient for PCP to form a swirl around the

Paneth cell, but is obviously a different mechanism than the later WNT3 to PCP coupling.

Paneth Cell Interactions				
Params	λ_1	λ_2	λ_3	λ_4
Value	0.5	0	0	0.5

Nearest Neighbour Interactions				
Params	λ_1	λ_2	λ_3	λ_4
Value	1	0	0	0

Table 4: **Parameter values used to create the images in Figure 27**. Note also that in this configuration, only the Paneth cell has special interactions with its neighbours. All other cells interact through the AB vectors only, though the sheet was initialized with PCP aligned for all cells.
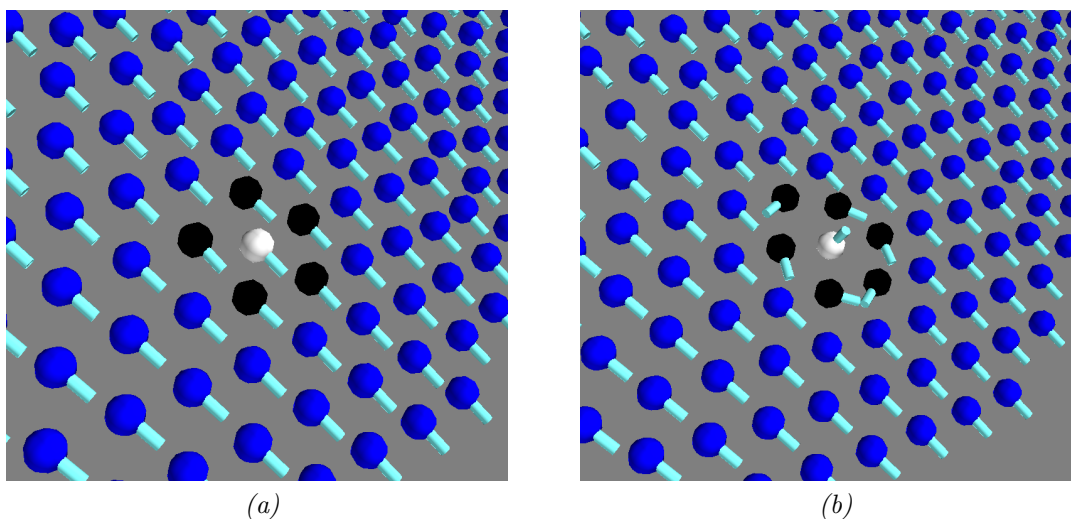

(a) (b)

Figure 27: **Formation of a stable swirl**. PCP vectors are represented as light nematic vectors. Paneth cell is white and nearest neighbours are black. (a) Initial configuration at 0 updates. (b) Simulation result after 10000 updates. Note that because of the nematic nature of the interactions, the bottom two black cells have opposing PCP vectors.

Figure 27 shows the system initialized in the plane and the effect of the PCP orientation mechanism. Note that I for consistency with the methods used in [13] keep $\sum_i \lambda_i = 1$. We are able to get a swirl and this is stable, since it does not distort or in other ways change over the course of ~ 9000 updates. For lower values of λ_4 I get that the swirl becomes less defined. Note also that the PCP vector of the Paneth cell points out of plane because of the shape of Eq. 19, which acts to make the PCP vector of the Paneth cell itself orthogonal to the distance vectors of all its neighbours.

43

Turning on λ_2 in the nearest neighbour interactions yields slightly different behaviour, as seen in Figure 28.

Paneth Cell Interactions				
Params	λ_1	λ_2	λ_3	λ_4
Value	0.5	0	0	0.5

Nearest Neighbour Interactions				
Params	λ_1	λ_2	λ_3	λ_4
Value	0.6	0.4	0	0

Table 5: **Parameter values used to create the images in Figure 28**.
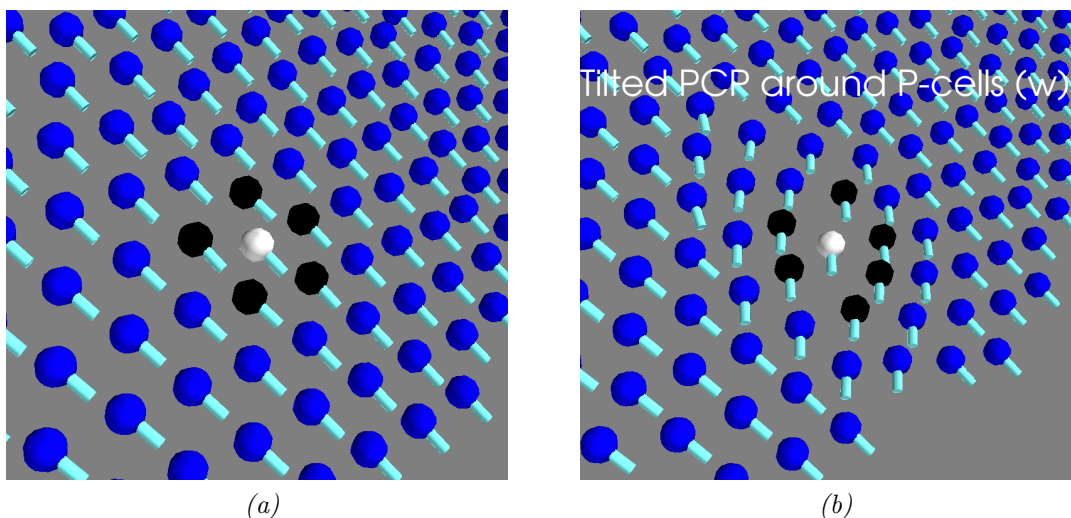
Figure 28: **Changing parameters**. (a) Initial configuration at 0 updates. (b) Result after 10000 updates.

The $\lambda_2 S_2$-term acts to shift PCP alignment. This resulting configuration in Figure 28 (b) is stable, since it also does not change for ~ 9000 updates. As λ_2 is lowered and comes close to 0, I regain the previous result and a swirl emerges. Roughly the same behaviour is observed if instead we vary λ_3 and keep $\lambda_2 = 0$.

4.1.1.2   Orienting PCP Through Non-Emergent WNT3 Gradients   Even though I am able to get a stable swirl in the previous section, we are not just interested in the nearest neighbours interacting with the Paneth cell. For a tube to grow, we know from [13, 11, 7] that many cells need to orient their PCP vectors in order to have emergent CE and budding out-of-plane.

As explained in the next sections and in the main text, I implemented several versions of a WNT3 gradient *field* where cells i have associated with them a scalar w_i based on this gradient field. To interact with this field, we introduced a gradient unit vector $\hat{G}_i$, associated to all cells i that are affected by the local gradient of WNT3 emanating from

44

the Paneth cell(s). As explained in the main text, we introduced a modified version of Eq. 18 with a change of the S_4 interaction:

$$S_4 = (\hat{q}_i \times \hat{G}_i) \cdot (\hat{q}_i \times \hat{G}_i) = 1 - (\hat{q}_i \cdot \hat{G}_i)^2 \tag{20}$$

with

$$\vec{G}_i = \sum_j (w_i + w_j) \cdot \hat{r}_{ij}. \tag{21}$$

The effect of this mechanism under different variants of the WNT3 gradient can be seen in the following paragraphs.

Linear WNT3 Gradient   Now, in the previous section we looked at the case of a single Paneth cell. I now turn our attention to the case where we instead look at a small cluster of several Paneth cells. With this, I define the first iteration of the WNT3 gradient as a decreasing linear function that is equal to 0 at a distance $r = 10$ from the center of mass of the Paneth cell cluster and maximum at the center of mass. The maximum value was chosen as $w_0 = 100$. The scalar weights w_i are then determined from the same function that generates the WNT3 gradient, i.e. from the distance $r_{i,cm}$ of the cells to the center of mass of the Paneth cell cluster. The closer the cell is to the cluster, the greater the weight. From this implementation we get a ring of neighbour cells about 4∼6 cells thick. As illustrated in Fig. 29, this mechanism also produces a PCP-swirl around the Paneth cell cluster. The configuration seen in Fig. 29 (a) is stable at $t = 5000$ updates, at which point the simulation ended. At this point the overall structure has not changed, and there is no budding out-of-plane. The configuration seen in Fig. 29 (b), however, is seen to begin bulging out after $t \approx 600$ updates for a different set of parameters. This progression[14] and the parameters used are shown in Fig. 30 and Fig. 31.

For these simulations the number of Paneth cells are held fixed at 7. Note that when either λ_2 or λ_3 are non-zero, then PCP of neighboring cells will align. In these images, all cells have all parameters non-zero except for the λ_4 interaction. This is only non-zero for the black cells, which are the only cells that have non-zero w_i's. Also noteworthy are the nematic topological defects, typically encountered in nematic crystal arrays, on either side of the black ring of cells. This is especially evident from Fig. 31 (a). These arise because of the nematic nature of the S_2 and S_3 terms in Eq. 18 and have been reviewed in the discussion.

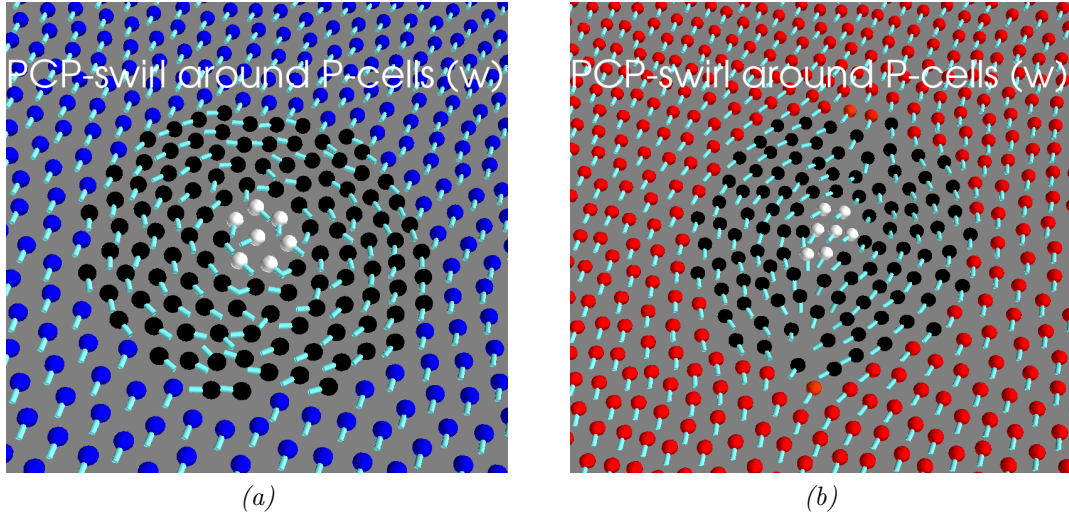[14]Animation of the protrusion forming at 8x playback speed: `https://youtu.be/cVLH-_6G53A`

Figure 29: **Formation of large swirl from linear gradient**. *(a) Configuration after 100 updates. Paneth cells are white and cells with $w_i > 0$ are black. Parameters $\lambda_1, \lambda_4 = 0.5$ and $\lambda_2, \lambda_3 = 0$. (b) Simulation result after 100 updates with parameters $\lambda_1 = 0.4$ and $\lambda_2, \lambda_3, \lambda_4 = 0.2$.*
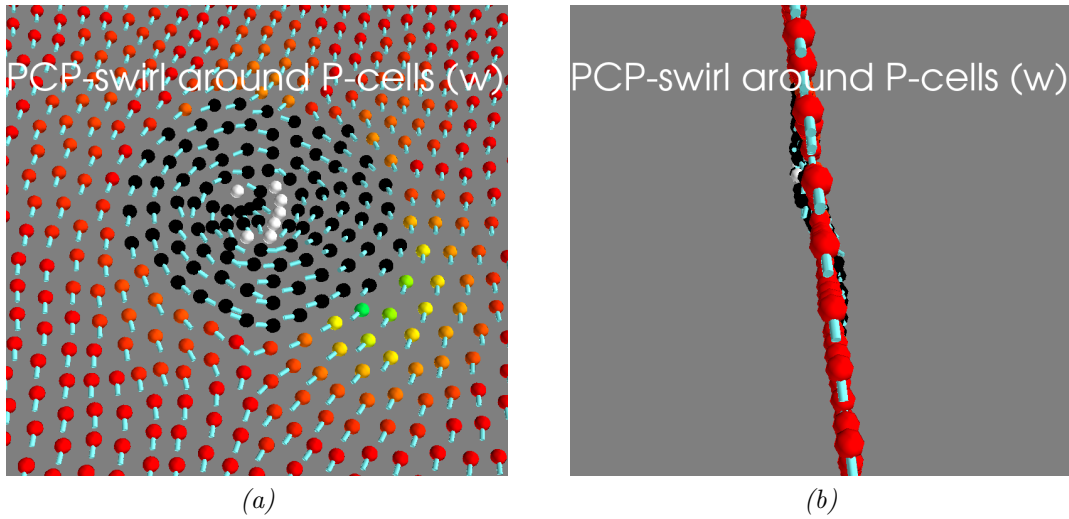

Figure 30: **Swirl starts budding out from plane with Paneth cells at the crypt base**. *(a) Top view of configuration after 600 updates. Paneth cells are white and cells with $w_i > 0$ are black. Same parameters as in (b) in Fig. 29. (b) Side view of the same configuration of cells. A slight bulging is seen on either side of the cell sheet.*
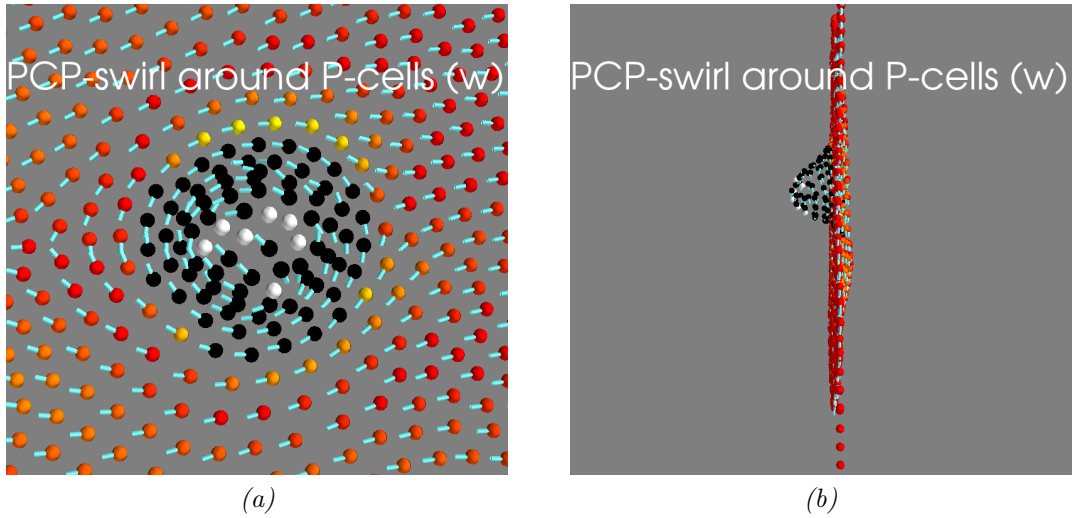
46

Figure 31: **Plane now shows clear budding out of plane**. *(a) Top view of configuration after 1500 updates. Same parameters as in (b) in Fig. 29. (b) Side view of the same configuration of cells. The bulging is now overwhelmingly on one side only, even though slight bulging in the opposite direction is still visible.*
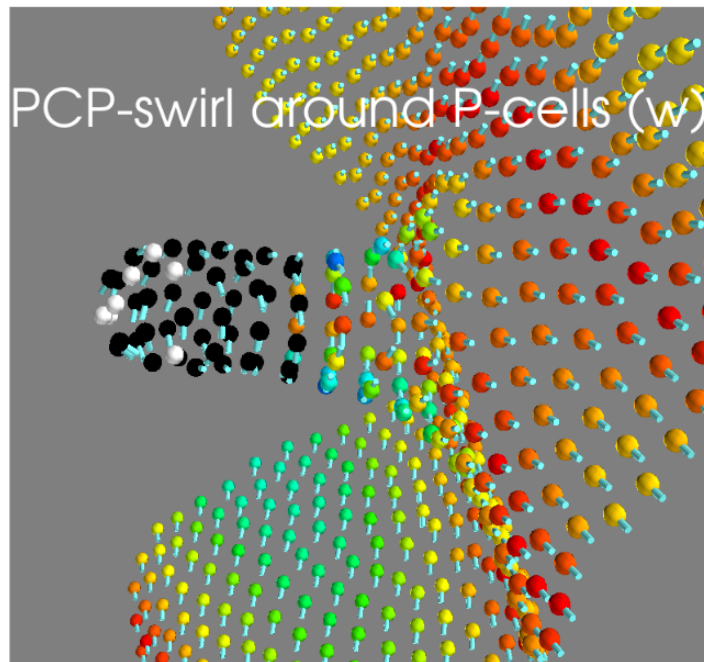

Figure 32: **Running the system up to** $t = 5000$ **steps yields an elongation of the protrusion**. *Note how the rest of the cell sheet warps and how the black ring of cells has followed the cluster of Paneth cells as the structure has elongated. The colors of the sheet are not of importance.*

47

Exponential WNT3 Gradient Thus far I have been able to generate a crypt-like protrusion from a linear, non-emergent gradient. What about a non-emergent exponentially decaying gradient, still emanating from the center of mass of the Paneth cell cluster? The authors in [3] find that the mechanism that is by far the most likely responsible for the establishment of a WNT3 gradient are the local cell divisions from the crypt stem cells. Such a mechanism would, in our view, likely result in an exponentially decreasing gradient of the form

$$w_i(r_{i,cm}) = \frac{w_0}{2^{r_{i,cm}}} \tag{22}$$

with $r_{i,cm}$ again being the radial distance from each individual cell to the center of mass of the cluster of Paneth cells, or, in the case of a single Paneth cell, the distance to this single cell. This is the reference function introduced in the main text. I find it of interest to directly check whether a global gradient of this form when imposed onto the system yields interesting behaviours. Eq. 22 is now the function by which we generate the w_i's, and we will use this as a reference to compare with the WNT3 gradients observed in simulations, also after adding proliferation from stem cells. For now, however, we do not implement cell divisions but choose to investigate this minimal system, as shown in Fig. 33.

Figure 33 shows the initial starting configuration and the resulting system. Note that this was only observed in **one** of the simulations. We have thus shown that it is possible, although very rare, for the model in this form to generate a crypt-villus structure. For this system, a gradient threshold has been introduced such that only cells[15] that have w_i's above this threshold interact though the S_4 mechanism. Even though this gradient threshold is implemented and working for one of the two protrusions, the initial budding of the Paneth cell cluster initiates a second budding area closeby in the opposite direction which itself organizes into a villus-like structure and elongates as the simulation progresses.

---

[15]This subset of interacting cells will from now on be referred to as the TA cells, representing the cells of the transit amplifying zone as shown in Figure 1.
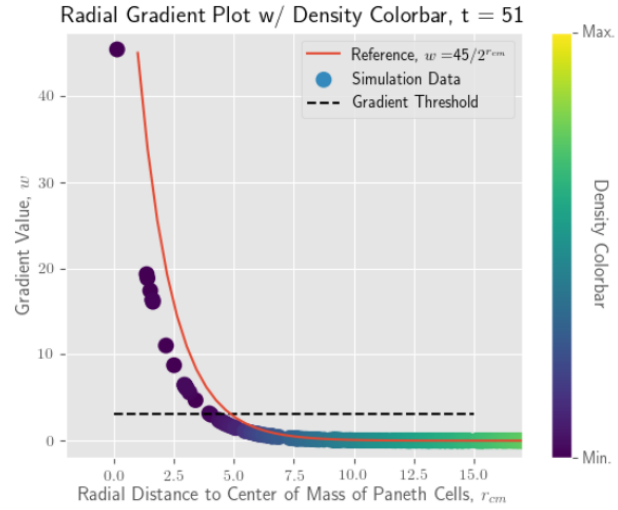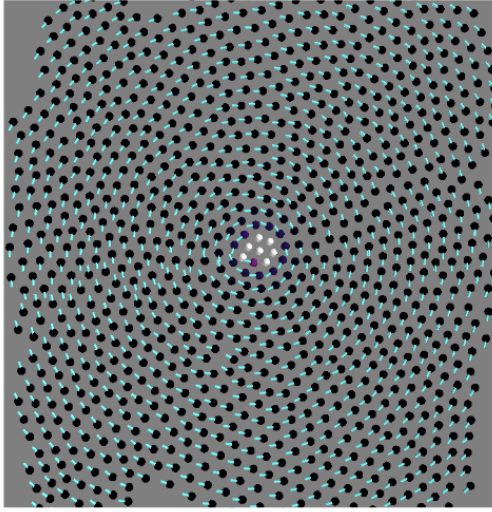
(a)
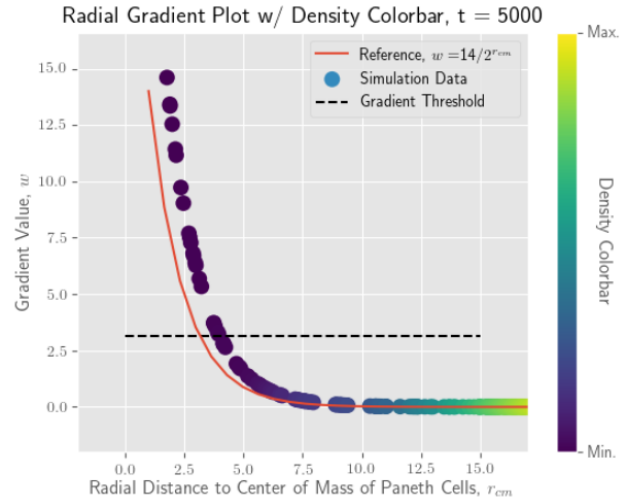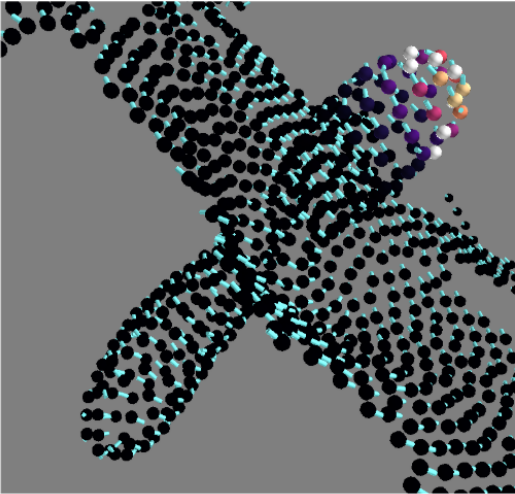
(b)

Figure 33: **Full villus-crypt structure has formed with the crypt niche represented by the white Paneth cells and colored cells that are above the gradient threshold and interact through the S_4 mechanism.** *(a) Configuration of the system at 51 steps after the entire cell sheet has organized itself such that PCP vectors swirl around the central Paneth cell cluster. (b) Resulting configuration after 5000 steps. Parameter set, globally: $\lambda_1 = 0.4$, $\lambda_2 = 0.2$, $\lambda_3 = 0.2$, $\lambda_4 = 0.2$ (λ_4 is for cells above gradient threshold only). This is a very rare outcome since it only happened once during the entire work.*

4.1.1.3 Emergent WNT3 Gradient from Cell Divisions Note that the linear and exponential gradients introduced in the previous section represent somewhat arbitrary choices for the w-field. *The main point of introducing these non-emergent gradient fields was to show that it is indeed possible to have a field-interaction produce swirls and protrusions out of plane* and even a crypt-villus pair in the case of the exponential, global gradient. However, as mentioned in the introduction, a more realistic approach is to have the WNT3 gradient emerge from local cell divisions from the stem cells in close contact with the Paneth cells in combination with a cell-cell contact mediated diffusion. Also, the exponential, global WNT3 gradient does not reflect the weak solubility of WNT3 that is reported in the literature[16].

Now, each cell is again assigned a scalar value w_i based on its local neighbourhood. This time, however, these are not assigned based on Eq. 22. Instead, the Paneth cells act as sources of WNT3 by always having their respective $w_i = w_0$, where again $w_0 = 100$. The stem cells are then assigned $w_i = w_0/2$ and this is ensured at each step in the simulation. This factor of $1/2$ just constitutes a choice that we made initially, but the denominator in Eq. 22 reflect that upon division we expect the concentration of available WNT3 for each cell given by the scalar w_i to decrease by a factor of $1/2$ as also reported for the dilution of surface-bound WNT3 due to cell divisions in [4]. I thus explicitly fix the w_i's of the two resulting cells from a cell division to half the value of the original cell before division. Furthermore I continue with the gradient threshold to help define the transit amplifying zone and thus determine which cells are allowed to act through the S_4 mechanism. I treat cell divisions as symmetric[17] single cell divisions at a range of division intervals. Figure 34 was generated with 200 steps between divisions from single stem cells. One cell from this subset of cells was chosen at random every 200 steps.

---

[16]For in-vivo intestinal systems the Paneth cells are not the sole sources of WNT, though. Mesenchymal cells in the surrounding tissue also generate a WNT2 gradient [4], and as such, the global gradient could still be of interest. However, we choose to continue by investigating proliferation from stem cells and the emergent WNT3 gradients.

[17]In the literature, the term *symmetric* cell divisions does not refer to the spatial aspects of division but rather on the properties of the newly divided cells. Symmetric division means that both resulting cells have the same properties as the original single cell, whereas asymmetric division means that the two resulting cells are different in terms of cell fate. In our case, symmetric divisions from stem cells means that the daughter cells themselves are stem cells if they meet the criteria for being a stem cell as discussed under *Determining Cell Stemness*.
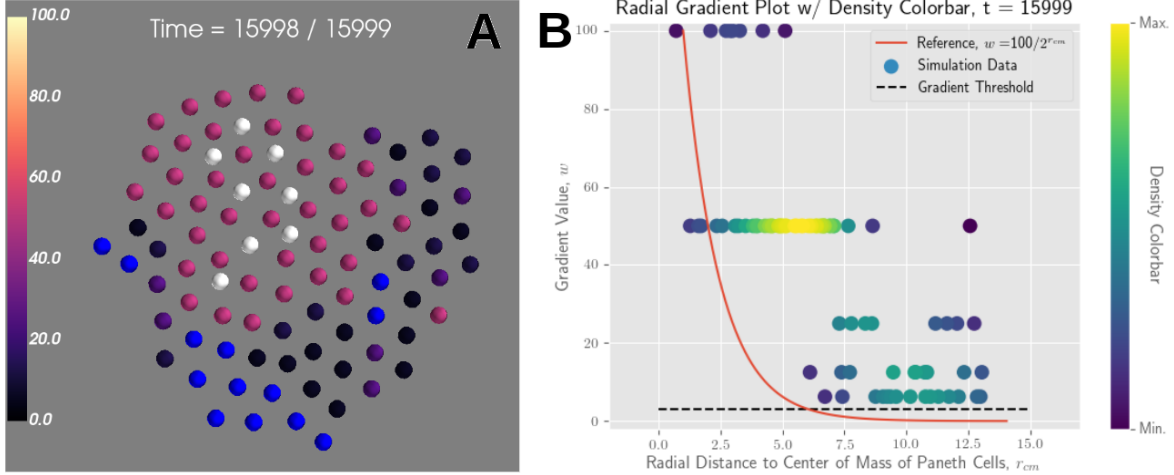
Figure 34: **WNT3 is not evenly distributed**. *Distribution of WNT3 gradient from an initial patch of 16 cells (8 of them Paneth cells) after 16000 steps, i.e. for 80 added cells. Note the two top rows on the gradient distribution plot in **B** representing the Paneth cells and the stem cells. The distinct rows of cells reflect the fact that upon cell divisions the w_i's are halved. Other simulations initiated with different random seeds yielded similar outcomes. **A** Blue cells have $w_i = 0$ and are not included in the distribution plot. These cells were during the first steps of the simulation not recognized as either stem cells or Paneth cells due to the initial configuration. These cells were therefore also never initialized with a non-zero w_i and thus also not treated as TA cells. Upon cell divisions from the stem cells these cells were then pushed to the boundary. The cells that were above gradient threshold but below the w_i stem cell level, i.e. $w_{threshold} \leq w_i < 50$, were treated as TA cells and these are represented by the bottom three rows on the gradient distribution plot. Same figure as in the main text.*

For clarification, TA cells are the cells that are not stem cells or Paneth cells and that are affected by the WNT3 gradient and above gradient threshold. Paneth cells and stem cells interact through the M-matrix, Eq. 15, which substitutes the S_1 interaction strength for these cells.

Directed Division   The configuration in Figure 34 was initialized from a small patch of cells in order to investigate how the minimal system would behave and how the resulting gradient would spread out. *The results illustrate cell divisions alone are not sufficient when used as the driving mechanism to spread the WNT3 gradient*, i.e. it does not resemble the decaying exponential reference. This is, however, even taking into account that newly created cells from cell proliferation are not positioned randomly when introduced into the plane, since the gradient distribution would then be even worse. Newly created cells were positioned through *directed division*.

This was motivated by the authors of [5] mentioning that one can manipulate the direction of stem cell divisions by influencing the local environment of an aggregate of embryonic stem cells with small beads treated with immobilized WNT proteins. For this reason I chose to let the direction of division in the simulations be determined by the gradient vector $\hat{G}_i$ of the proliferating cell such that the newly added cell is placed a unit distance away in the direction of this gradient. Furthermore I chose to fix the gradient vectors $\hat{G}_i$ such that they are positioned in the local cell plane, i.e. orthogonal to the AB vectors, such that divisions occur in-plane as indicated also in Figure 1 since this also was seen to be beneficial to the distribution of the WNT3 gradient.

Determining Cell Stemness   For the introduction of proliferating stem cells I first needed to define what makes a stem cell, i.e. what determines cell stemness. I came up with three different mechanisms to define which cells are stem cells, of which two seemed to work well. First, stem cells are defined as the unique set of cells that are nearest Voronoi-neighbours to the cluster of Paneth cells, i.e. a stem cell is a cell that has at least 1 Paneth cell as a Voronoi-neighbour. Additionally, I demand that the fraction of stem cells and Paneth cells out of the total neighbourhood of the cell in question is greater than or equal to a given threshold, throughout the work chosen as 60%. These two mechanisms together ensure a stable number of stem cells in the crypt niche when run every 50 steps, i.e. the cell type check occurs every 50 steps. The third mechanism relied on determining cell stemness from the local concentration of WNT3, but this method turned out to be very sensitive to small changes in the way in which the gradient propagates and was subsequently put aside.

4.1.1.4   Isotropic Apical-Basal Constriction   It is known in the literature [22, 12] that constriction of the apical or basal surface of cells in developing epithelium plays a major role in the morphological development, whether it being in e.g. tube formation and closure or wound healing. For this reason, I chose to also implement AB isotropic constriction of the Paneth cells and their Voronoi-neighbourhood, as it is also indicated that Paneth cells are constricted (or as I call it in the main text, *wedged*) in Figure 6.
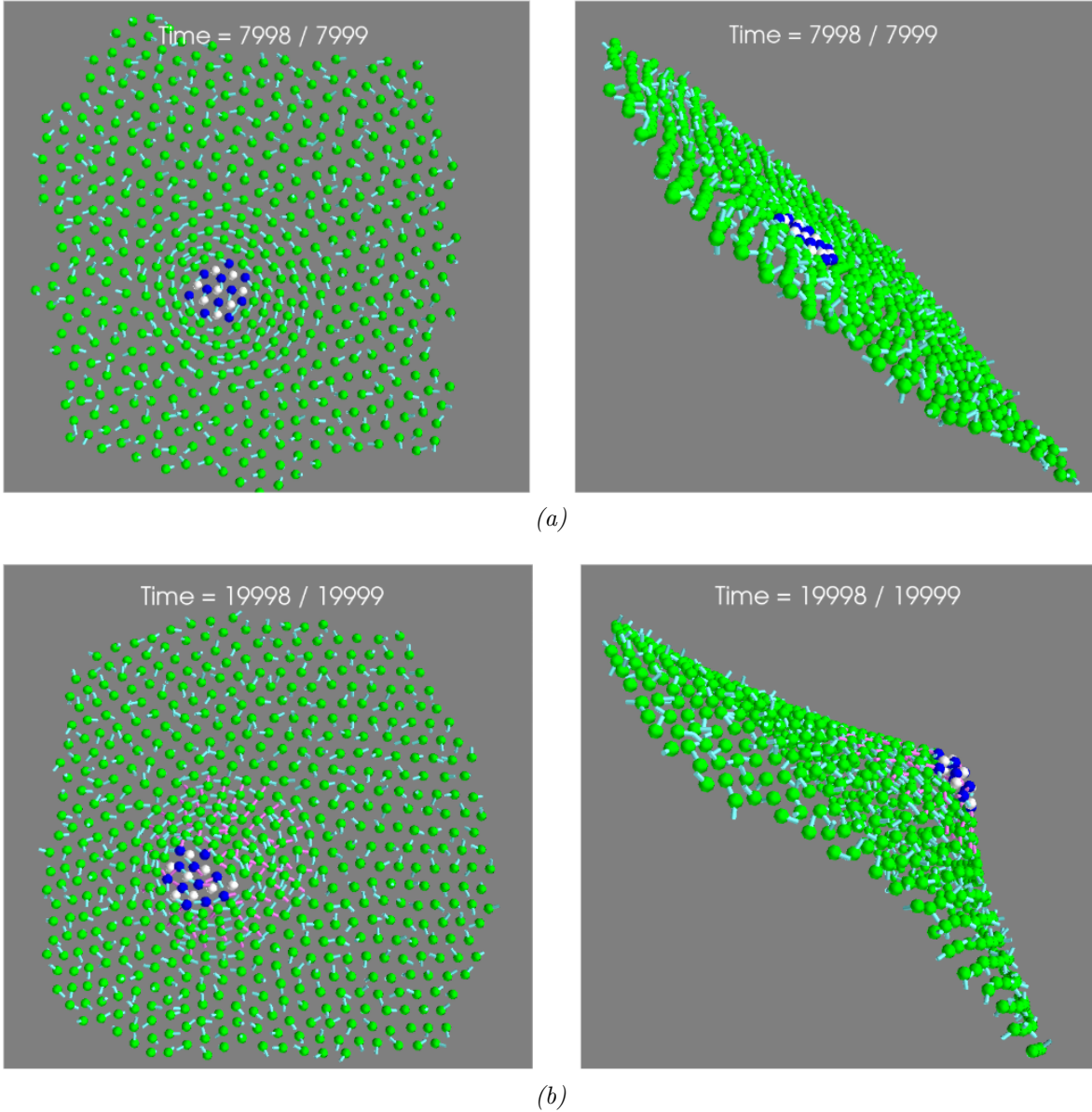
Figure 35: **With the new mechanisms, isotropic wedging of the Paneth cell to its surroundings helps budding out of plane**. (a) Left: Configuration of the system at 8000 steps, seen from a top view. Right: Same system seen from the side. Note that no protrusions have formed. Running the system for considerably longer does not change the morphology. All mechanisms active, gradient vectors have just not been shown for illustrative purposes. (b) Same initial configuration but now including isotropic wedging of the Paneth cells. Note that I now see that a protrusion is starting to take form. Also in this image, the gradient vectors $\hat{G}_i$ have been plotted. Note that in both configurations, PCP interactions through either S_2, S_3 or S_4 have not been activated. Only cells that have w_i's above threshold interact through the whole of Eq. 18. Parameters for TA cells; $\lambda_1, \lambda_2, \lambda_3, \lambda_4 = 1.0, 0.2, 0.1, 0.2$.

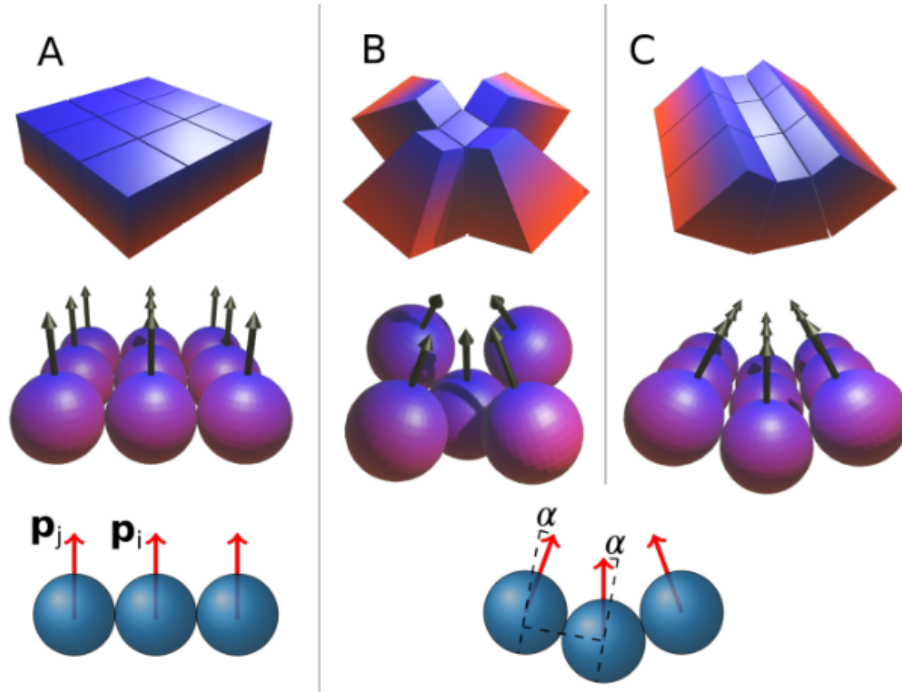I chose to implement it as the authors did in [11], as illustrated in Figure 36.

*Figure 36: **Schematic illustrating different examples of wedging**. From [11], Nielsen et al., 2020. In this work, I use $\alpha = 0.5$ as in [11] for all simulations and isotropic wedging as illustrated in **B**. For the case **A** the parameter $\alpha = 0$. Case **C** shows anisotropic wedging.*

Wedging is introduced by substituting the AB vector of cell i with a modified AB vector according to

$$\hat{p}_{i,new} = \frac{p_i - \alpha \hat{r}_{ij}}{|p_i - \alpha \hat{r}_{ij}|} \tag{23}$$

with the constant α determining the strength of the wedging.

Looking at Fig. 35, it is especially important that the mixed patch of Paneth and stem cells is seen to be intact even after 20.000 steps and in Fig. 9 after 10.000 steps, i.e. the patches are stable.

4.2 Stability of Stem Cell Niche

The figures and plots in this section aim to illustrate how the stability of the stem cell niche evolves over time when one has cell divisions from stem cells. I evaluate the stability by computing the average fraction of similar neighbours as a function of simulation steps for 5 different stem cell division rates. The divisions are happening every 50, 100, 200, 300 and 400 steps. I also show the specific configuration of cells for comparison. Parameters in the M-matrix for differential adhesion are the same as stated in the main text.

In all cases, the original configuration (patch) of stem cells and Paneth cells change over time and for the fastest division rates the patches tend to break apart and form smaller sub-patches. For the slower division rates the patches tend to not break apart but instead become rather string-like and elongated. These are most likely the energetically most favorable and stable configurations since I often see these structures. In this work I end up choosing 200 steps between divisions from randomly chosen stem cells (not to be confused with the stem cell cycle) since this seems to be the point between string-like structures and patches breaking apart.

For all plots, I let the simulations run up until 80 cells have been added to the system from stem cell divisions.
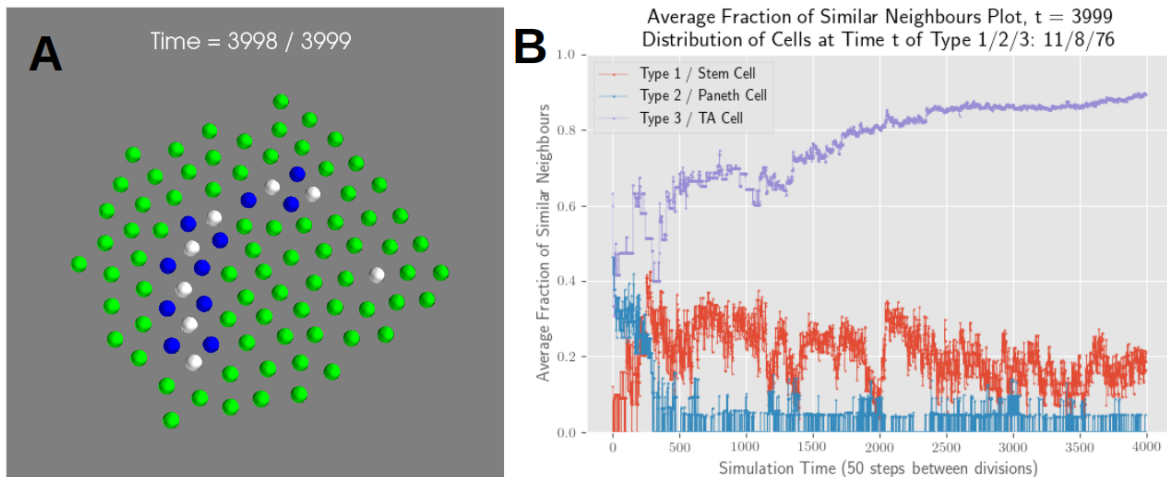

Figure 37: ***A) Crypt niche breaks apart and B) fractional neighbour plot shows clear fluctuations for the stem cells. 50 steps between divisions.***
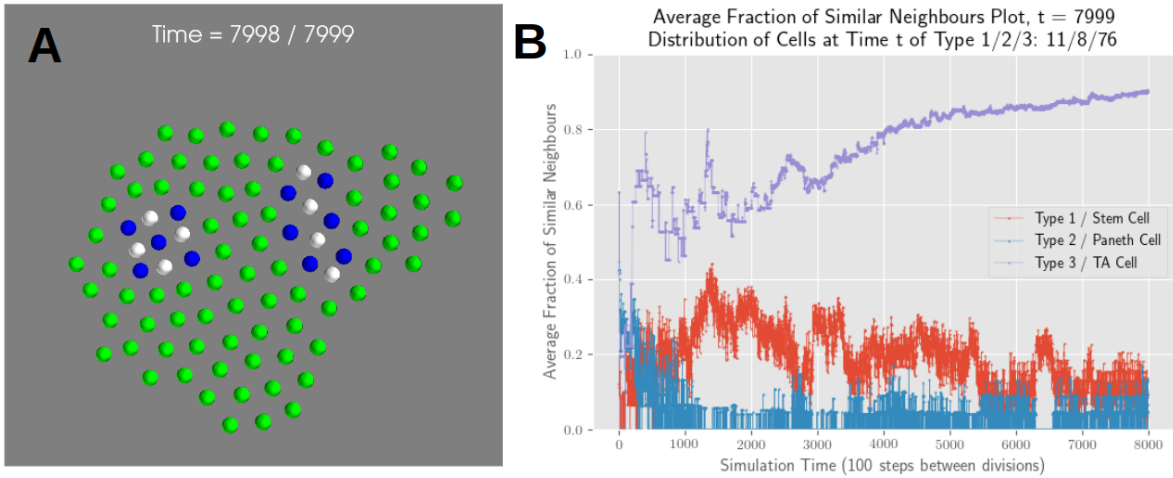
Figure 38: **A) Crypt niche breaks apart and B) fractional neighbour plot shows clear fluctuations for the stem cells. 100 steps between divisions.**
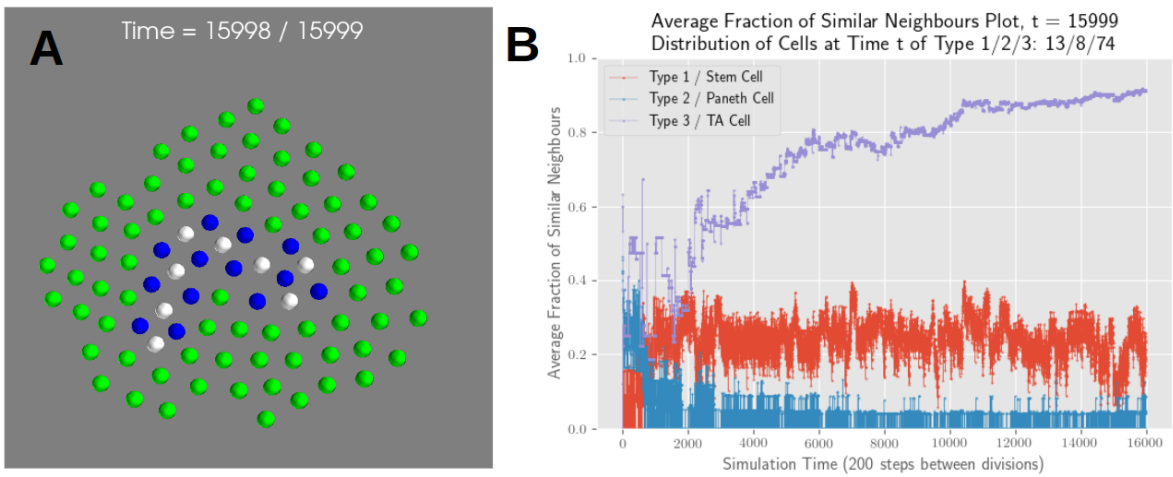

Figure 39: **A) Crypt niche remains intact. B) Fractional neighbour plot shows more stable neighbourhood for the stem cells. 200 steps between divisions.**
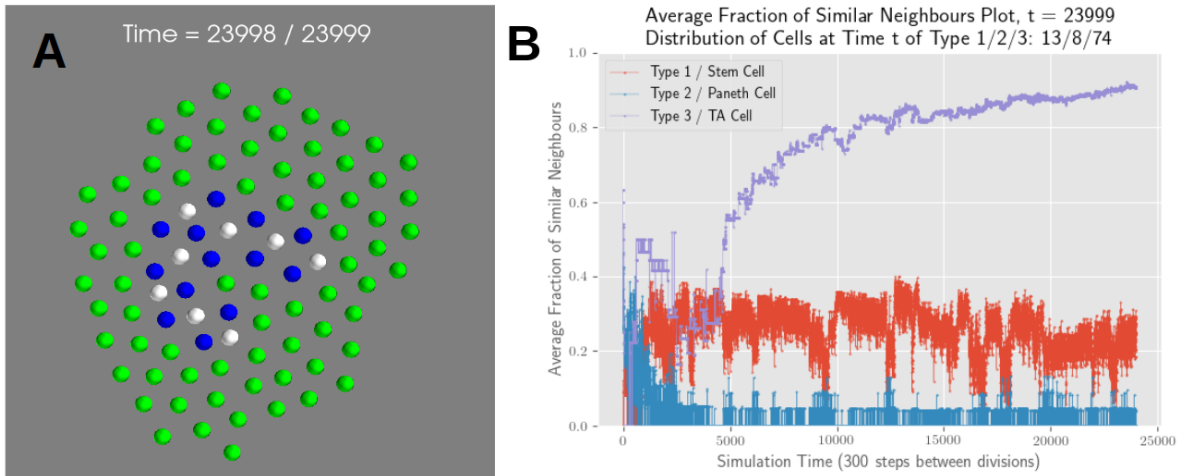
Figure 40: **A) Crypt niche remains intact. B) Fractional neighbour plot shows more stable neighbourhood for the stem cells. 300 steps between divisions.**
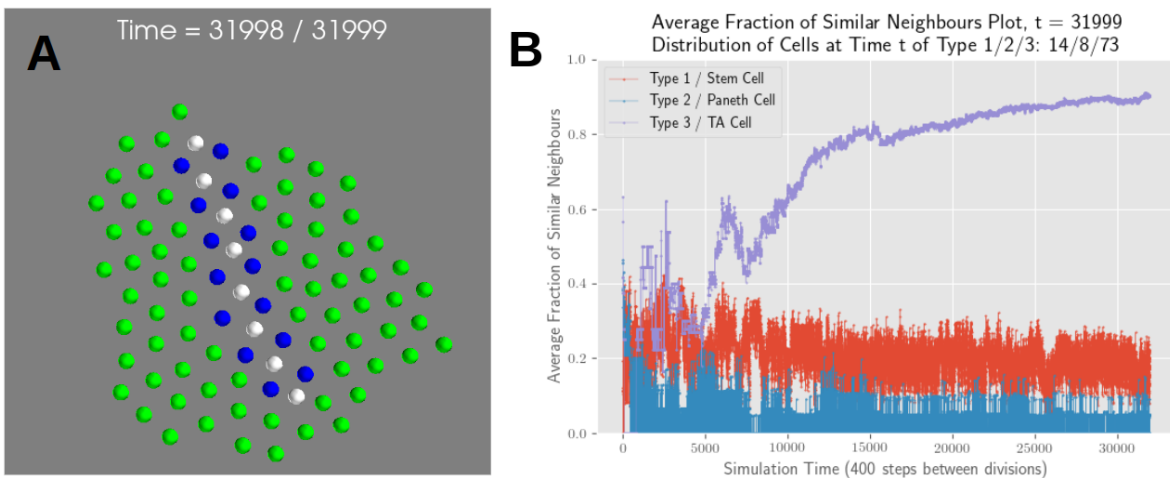

Figure 41: **A) Crypt niche remains intact, though elongated. B) Fractional neighbour plot shows even more stable neighbourhood for the stem cells. 400 steps between divisions.**

4.3 Parameter Scan for Different Random Seeds

This section introduces the results from additional OAT parameter sensitivity scans. The scans are done in the same manner as in the main text but for different random seeds, 3 extra in total corresponding to 240 additional simulations. This was done to ensure that the reported behaviour in the main text did not change considerably when changing the random seed.

Value	0.05	0.10	0.15	0.20	0.25	0.30	0.35	0.40	0.45	0.50
λ_1	✗	(✓)	(✓)	(✓)	(✓)	(✓)	(✓)	(✓)	(✓)	(✓)
λ_2	✗	✓	✓	✓	✓	(✓)	(✓)	(✓)	(✓)	(✓)
λ_3	✓	✓	(✓)	✗	✗	✗	✗	✗	✗	✗
λ_4	✓	✓	✓	✓	✓	✓	✓	✓	✓	✓

Value	0.55	0.60	0.65	0.70	0.75	0.80	0.85	0.90	0.95	1.00
λ_1	✓	✓	✓	✓	✓	✓	✓	✗	✓	✗
λ_2	(✓)	(✓)	(✓)	✗	(✓)	(✓)	(✓)	(✓)	✗	✗
λ_3	✗	✗	✗	✗	✗	✗	✗	✗	✗	✗
λ_4	✓	✓	✓	✓	✓	✓	✓	✓	✓	✓

Table 6: **Parameter sensitivity analysis from working set of parameters, random seed is 4.**

Value	0.05	0.10	0.15	0.20	0.25	0.30	0.35	0.40	0.45	0.50
λ_1	✗	(✓)	(✓)	(✓)	(✓)	(✓)	(✓)	(✓)	(✓)	✓
λ_2	✗	✓	✓	✓	✓	(✓)	(✓)	(✓)	(✓)	(✓)
λ_3	✓	✓	✗	✗	✗	✗	✗	✗	✗	✗
λ_4	✗	✓	✓	✓	✓	✓	✓	✓	✓	✓

Value	0.55	0.60	0.65	0.70	0.75	0.80	0.85	0.90	0.95	1.00
λ_1	✓	✓	✓	✓	✓	✓	✓	✓	✗	✗
λ_2	(✓)	(✓)	(✓)	(✓)	(✓)	✗	(✓)	(✓)	✗	✗
λ_3	✗	✗	✗	✗	✗	✗	✗	✗	✗	✗
λ_4	✓	✓	✓	✓	✓	✓	✓	✓	✓	✓

Table 7: **Parameter sensitivity analysis from working set of parameters, random seed is 13.**

For λ_4 parameter in Table 6 the structures do not break apart in the high parameter values but instead do not qualitatively resemble crypts, which is also true for the very

low values. I do however choose to include these for further analysis. Table 7 is the same parameter scan for random seed set to 13.

Below are the results for random seed set to 5.

Value	0.05	0.10	0.15	0.20	0.25	0.30	0.35	0.40	0.45	0.50
λ_1	✗	✗	(✓)	(✓)	(✓)	(✓)	(✓)	(✓)	(✓)	(✓)
λ_2	(✓)	✓	✓	✓	✓	(✓)	(✓)	(✓)	(✓)	(✓)
λ_3	✓	✓	✗	✗	✗	✗	✗	✗	✗	✗
λ_4	✓	✓	✓	✓	✓	✓	✓	✓	✓	✓

Value	0.55	0.60	0.65	0.70	0.75	0.80	0.85	0.90	0.95	1.00
λ_1	(✓)	✓	✓	✓	✓	✓	✓	✓	✗	✗
λ_2	(✓)	(✓)	(✓)	(✓)	(✓)	(✓)	✗	✗	✗	✗
λ_3	✗	✗	✗	✗	✗	✗	✗	✗	✗	✗
λ_4	✓	✓	✓	✓	✓	✓	✓	✓	✓	✓

*Table 8: **Parameter sensitivity analysis from working set of parameters, random seed is 5**.*

To summarize, here are all working parameter regimes from the different parameter scans presented side by side for comparison for seeds 42, 4, 13 and 5.

$\lambda_1 \in [0.45; 0.90]$ $\lambda_1 \in [0.55; 0.95]$ $\lambda_1 \in [0.50; 0.90]$ $\lambda_1 \in [0.60; 0.90]$

$\lambda_2 \in [0.10; 0.30]$ $\lambda_2 \in [0.10; 0.25]$ $\lambda_2 \in [0.10; 0.25]$ $\lambda_2 \in [0.10; 0.25]$

$\lambda_3 \in [0.05; 0.10]$ $\lambda_3 \in [0.05; 0.10]$ $\lambda_3 \in [0.05; 0.10]$ $\lambda_3 \in [0.05; 0.10]$

$\lambda_4 \in [0.05; 1.00]$ $\lambda_4 \in [0.05; 1.00]$ $\lambda_4 \in [0.10; 1.00]$ $\lambda_4 \in [0.05; 1.00]$

I note that the parameter regimes in which the simulations yield emergent, successful crypt formation do not change considerably when changing the random seeds used for simulations. The rate of successful crypt formation, taken as an average over all parameter scans, is 42%.

4.4 Estimation of Crypt Metrics

In order to estimate the height, width and volume of the crypts I chose to use an approach taking inspiration from a former Master student of my supervisor, Sigurd Carlsen.
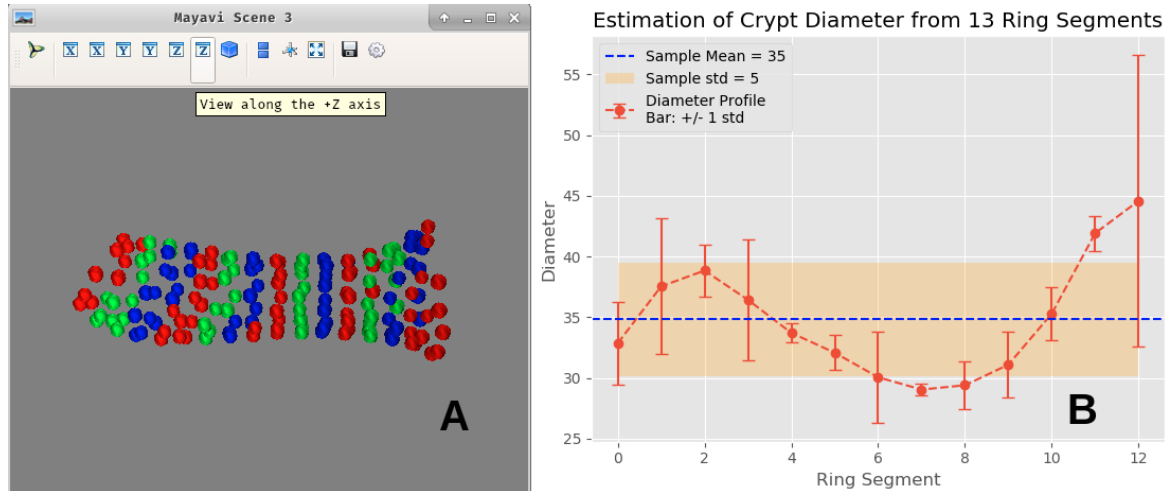

Figure 42: **Estimation of crypt diameter from ring segments**, *Subfigure* **A**. *In this scheme, one divides the crypts from simulations into ring segments down the crypt axis starting from the Paneth cell at the crypt tip. This is done using a spherical search algorithm starting from half the equilibrium distance away from the Paneth cell and then expanding this spherical shell in radial steps of the equilibrium distance, counting the cells in that particular shell and then saving these cells as a ring segment. Subfigure* **B**: *The large deviation on the last ring segment is due to the fact that the cells in the last segment in Subfigure* **A** *do not form a fully closed circle. Diameter in μm.*

Crypt Width From these ring segments one is then able to compute the radius (and thus diameter) of each ring segment of the crypt by taking the distance of the cells in the ring segment to the centre of mass of that ring segment and then taking an average of these distances. One then gets a profile of the diameter as a function of distance (or, equivalently, as a function of the ring segments) and the crypt width is then computed as the mean of the diameters of all the ring segments. Figure 42 shows an example of a set of ring segments from a crypt and the corresponding diameter profile. Note that for all segmentations, the Paneth cell and stem cells have not been taken into account. It is worth noting that this method is just one way of estimating the crypt diameter and it certainly has its pitfalls. For instance, if the crypt is very curved, or if the Paneth cell is not at the tip of the crypt, the ring segments do not correctly capture the diameter profile. On the other hand, this method proved easy to understand and fast to implement, as opposed to other methods where one searches for oppositely oriented AB vectors.

60

Crypt Height, Volume and Number of Cells   The same method can be expanded slightly to also yield an estimate of the height and volume of the crypts. A simple count can be done at the same time to get the number of cells in the crypt as well.

For the height, one can simply take the total number of ring segments and multiply by the inter-particle equilibrium distance and thus get a quick estimate. Another method is to take the centre of mass distance from the last ring segments to the Paneth cell. This again works best for straight crypts as in the example. These two methods vary slightly in their results, so I decided to take an average of the two estimates as the final estimate on the crypt height. The volumes are computed in a similar manner. I treat each ring segment as a slice of a solid cylinder and then add these up according to the number of ring segments. Again, the height of the individual cylinders is given as the inter-particle equilibrium distance. Figure 44 shows volume of crypts for all random seeds.

Effect of Changing the Inter-Particle Equilibrium Distance   When I in the main text introduce the working set of parameters as given in Tables 1 and 2, I implicitly allow for a change in the inter-particle equilibrium distance since now for these parameters $\sum_i \lambda_i > 1$. This might have an effect on the evaluated metrics, since for the results in the main text I used the equilibrium distance of 2 unit distances when computing crypt height, width, etc. For this reason I have chosen to compute the inter-particle distance and redo the metrics plot as shown in Figure 43. Using the parameters from Tables 1, 2, the new equilibrium distance is 1.76 as opposed to 2.
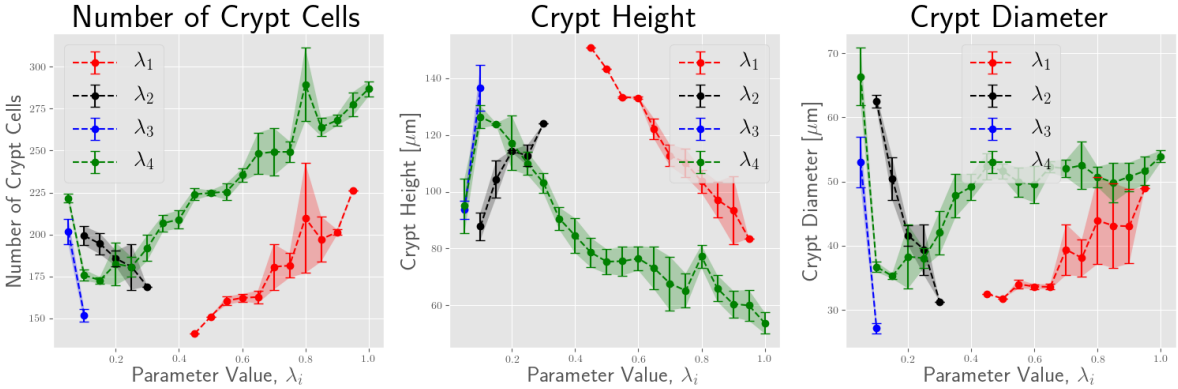

Figure 43: ***Taking into account a different inter-particle equilibrium distance yields almost identical results as in Figure 23.***
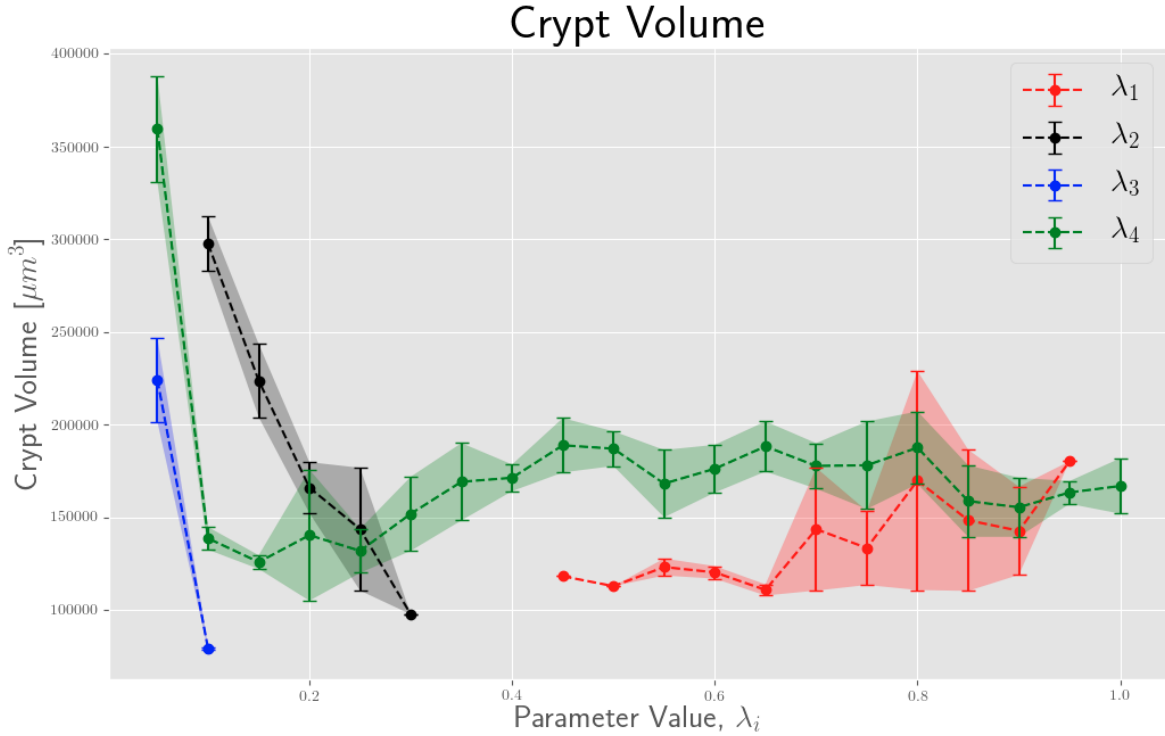
61

Figure 44: ***Crypt volume as function of parameter value***. *Clear trends are seen with low parameter value for λ_2, λ_3 and λ_4, where an initial decline in volume is observed. Volume stabilizes for λ_4 after about 0.4. For λ_1 the volume does not change considerably but an increase in the sample standard deviation is observed. Volume is computed at end of simulations, i.e. at 30.000 steps or roughly 7 days using the estimate of 12 hours for stem cell cycle. If instead we use the higher estimate for stem cell cycles of 32 hours, growth time is roughly 19 days. It is worth to note that the volume seem to behave in a similar manner as tube diameter when increasing λ_2 and λ_3, as also shown in Figure 23. The data points are sample averages over all random seeds used with errorbars equal to 1 sample standard deviation. Very small errorbars are due to the fact that only one data point was obtained for that sample for that particular parameter value. This means that only one of the 4 simulations using different random seeds yielded successful crypt formation. As such, a maximum of 4 values go into each data point. Some data points may however also just be very close to each other.*

4.5 WNT3 Gradient Propagation

In this section I report the ability of the crypts to grow when the time between the cell-cell contact diffusion computations is increased from 200 up to more than 800 steps, after which the crypts no longer grow. Data was collected after 30.000 steps. The reason that the plot title says 2999 steps is due to the fact that I save every 3000 steps, and as such I generate 10 files for each simulation. These plots are then generated for the last save file out of those ten save files.
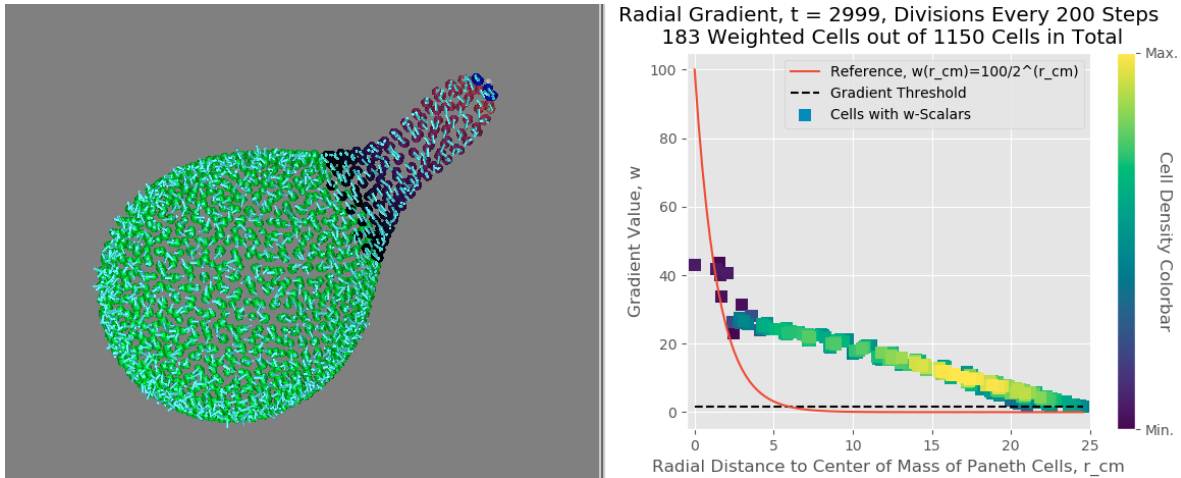

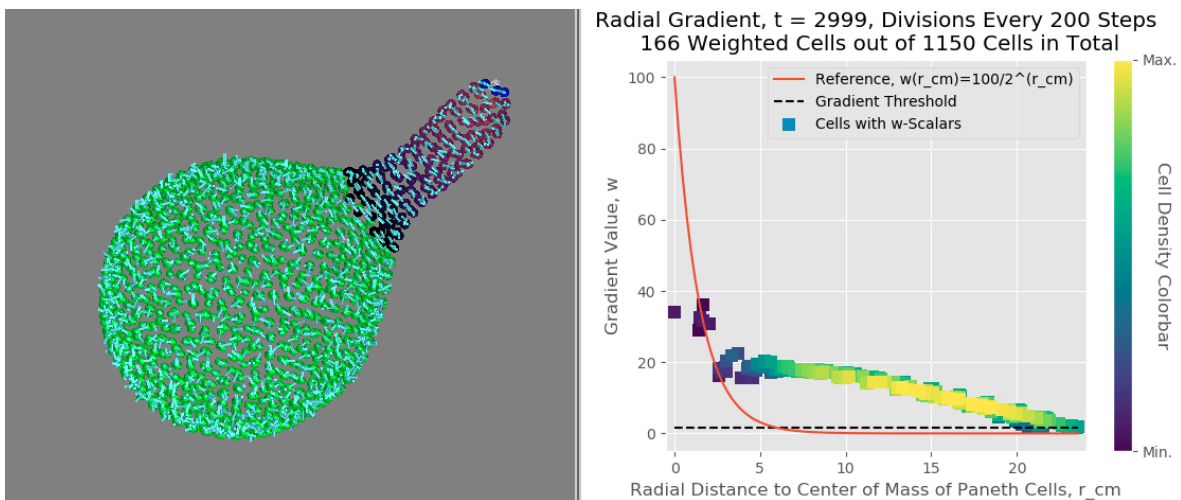*Figure 45:* **Crypt growth is still possible for 400 steps between cell-cell contact diffusion.**

Figure 46: **Crypt growth is still possible for 600 steps between cell-cell contact diffusion.**
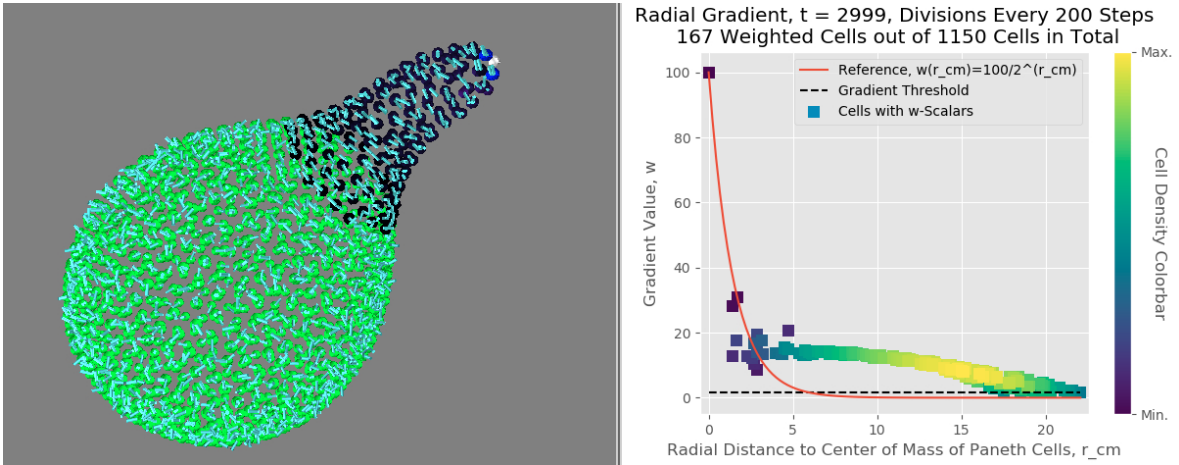
Figure 47: **Crypt growth is still possible for 800 steps between cell-cell contact diffusion.**
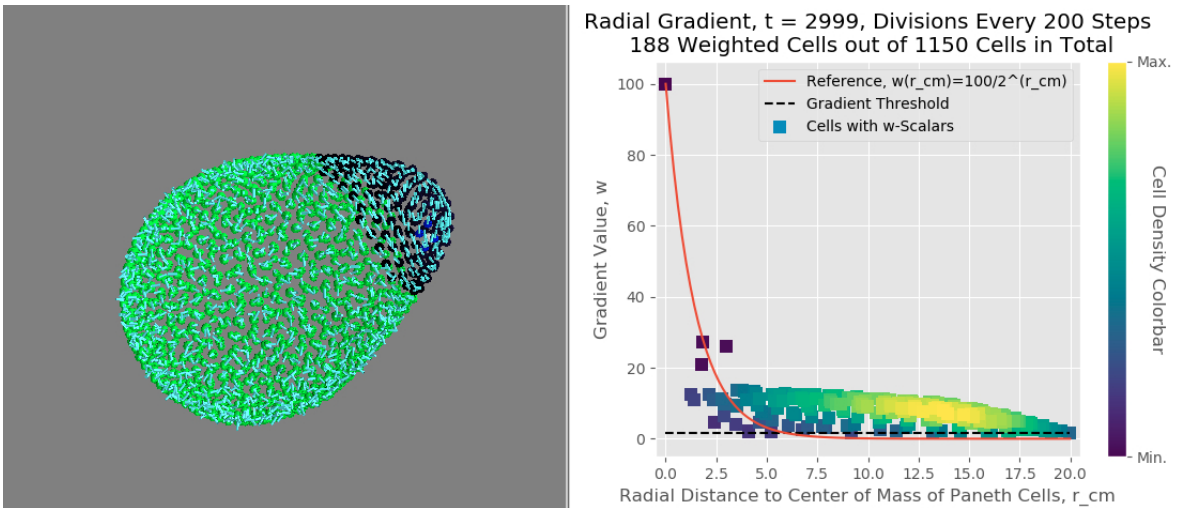

Figure 48: **Crypt growth is no longer possible for 900 steps between cell-cell contact diffusion.** *Organoid is seen to stay mostly spherical up to t = 30.000 steps. For 1000 steps and above between contact diffusion the crypts do not form protrusions at all.*

References

[1] Peter Buske, Jörg Galle, Nick Barker, Gabriela Aust, Hans Clevers, and Markus Loeffler. A comprehensive model of the spatio-temporal stem cell and tissue organisation in the intestinal crypt. *PLoS Computational Biology*, 7(1), 2011.

[2] Hazel Cheng and Matthew Bjerknes. Whole population cell kinetics and postnatal development of the mouse intestinal epithelium. *The Anatomical Record*, 211(4):420–426, 1985.

[3] Henner F. Farin, Ingrid Jordens, Mohammed H. Mosa, Onur Basak, Jeroen Korving, Daniele V.F. Tauriello, Karin De Punder, Stephane Angers, Peter J. Peters, Madelon M. Maurice, and Hans Clevers. Visualization of a short-range Wnt gradient in the intestinal stem-cell niche. *Nature*, 530(7590):340–343, 2016.

[4] Helmuth Gehart and Hans Clevers. Tales from the crypt: new insights into intestinal stem cells. *Nature Reviews Gastroenterology and Hepatology*, 16(1):19–34, 2019.

[5] Shukry J. Habib, Bi Chang Chen, Feng Chiao Tsai, Konstantinos Anastassiadis, Tobias Meyer, Eric Betzig, and Roel Nusse. A localized Wnt signal orients asymmetric stem cell division in vitro. *Science*, 339(6126):1445–1448, mar 2013.

[6] Ashley Ceinwen Humphries and Marek Mlodzik. From instruction to output: Wnt/PCP signaling in development and cancer. *Current Opinion in Cell Biology*, 51:110–116, 2018.

[7] Julius B. Kirkegaard, Bjarke F. Nielsen, Ala Trusina, and Kim Sneppen. Self-assembly, buckling and density-invariant growth of three-dimensional vascular networks. *Journal of the Royal Society Interface*, 16(159):20190517, oct 2019.

[8] Denis Krndija, Fatima El Marjou, Boris Guirao, Sophie Richon, Olivier Leroy, Yohanns Bellaiche, Edouard Hannezo, and Danijela Matic Vignjevic. Active cell migration is critical for steady-state epithelial turnover in the gut. *Science*, 365(6454):705–710, 2019.

[9] Alistair J. Langlands, Axel A. Almet, Paul L. Appleton, Ian P. Newton, James M. Osborne, and Inke S. Näthke. Paneth Cell-Rich Regions Separated by a Cluster of Lgr5+ Cells Initiate Crypt Fission in the Intestinal Stem Cell Niche. *PLoS Biology*, 14(6):1–31, 2016.

[10] Sebastian R. Merker, Jürgen Weitz, and Daniel E. Stange. Gastrointestinal organoids: How they gut it out. *Developmental Biology*, 420(2):239–250, 2016.

[11] Bjarke Frost Nielsen, Silas Boye Nissen, Kim Sneppen, Joachim Mathiesen, and Ala Trusina. Model to link cell shape and polarity with organogenesis. *iScience*, page 100830, 2020.

[12] Tamako Nishimura, Hisao Honda, and Masatoshi Takeichi. Planar cell polarity links axes of spatial dynamics in neural-tube closure. *Cell*, 149(5):1084–1097, 2012.

[13] Silas Boye Nissen, Steven Rønhild, Ala Trusina, and Kim Sneppen. Theoretical tool bridging cell polarities with development of robust morphologies. *eLife*, 7:1–25, 2018.

[14] C. S. Potten and M. Loeffler. Stem cells: Attributes, cycles, spirals, pitfalls and uncertainties. Lessons for and from the crypt. *Development*, 110(4):1001–1020, 1990.

[15] Toshiro Sato, Robert G. Vries, Hugo J. Snippert, Marc Van De Wetering, Nick Barker, Daniel E. Stange, Johan H. Van Es, Arie Abo, Pekka Kujala, Peter J. Peters, and Hans Clevers. Single Lgr5 stem cells build crypt-villus structures in vitro without a mesenchymal niche. *Nature*, 459(7244):262–265, 2009.

[16] Thuan Beng Saw, Amin Doostmohammadi, Vincent Nier, Leyla Kocgozlu, Sumesh Thampi, Yusuke Toyama, Philippe Marcq, Chwee Teck Lim, Julia M. Yeomans, and Benoit Ladoux. Topological defects in epithelia govern cell death and extrusion. *Nature*, 544(7649):212–216, 2017.

[17] Arnout Schepers and Hans Clevers. Wnt signaling, stem cells, and cancer of the gastrointestinal tract. *Cold Spring Harbor Perspectives in Biology*, 4(4):1–14, 2012.

[18] Denise Serra, Urs Mayr, Andrea Boni, Ilya Lukonin, Markus Rempfler, Ludivine Challet Meylan, Michael B. Stadler, Petr Strnad, Panagiotis Papasaikas, Dario Vischi, Annick Waldt, Guglielmo Roma, and Prisca Liberali. Self-organization and symmetry breaking in intestinal organoid development. *Nature*, 569(7754):66–72, 2019.

[19] Hugo J. Snippert, Laurens G. van der Flier, Toshiro Sato, Johan H. van Es, Maaike van den Born, Carla Kroon-Veenboer, Nick Barker, Allon M. Klein, Jacco van Rheenen, Benjamin D. Simons, and Hans Clevers. Intestinal crypt homeostasis results from neutral competition between symmetrically dividing Lgr5 stem cells. *Cell*, 143(1):134–144, 2010.

[20] Lilianna Solnica-Krezel. Conserved patterns of cell movements during vertebrate gastrulation. *Current Biology*, 15(6):213–228, 2005.

[21] Torsten Thalheim, Marianne Quaas, Maria Herberg, Ulf Dietrich Braumann, Christiane Kerner, Markus Loeffler, Gabriela Aust, and Joerg Galle. Linking stem cell function and growth pattern of intestinal organoids. *Developmental Biology*, 433(2):254–261, 2018.

[22] Mike R. Visetsouk, Elizabeth J. Falat, Ryan J. Garde, Jennifer L. Wendlick, and Jennifer H. Gutzman. Basal epithelial tissue folding is mediated by differential regulation of microtubules. *Development (Cambridge)*, 145(22):1–12, 2018.